INSTITUTE OF PHYSICS PUBLISHING WAVES IN RANDOM MEDIA

Waves Random Media **13** (2003) R1–R39 PII: S0959-7174(03)39997-5

TOPICAL REVIEW

Lasing in random media

Hui Cao

Department of Physics and Astronomy, Northwestern University, Evanston, IL 60208, USA

E-mail: h-cao@northwestern.edu

Received 3 February 2003
Published 18 June 2003
Online at stacks.iop.org/WRM/13/R1

Abstract

A random laser is a non-conventional laser whose feedback mechanism is based on disorder-induced light scattering. Depending on whether the feedback supplied by scattering is intensity feedback or amplitude feedback, random lasers are classified into two categories: random lasers with incoherent feedback and random lasers with coherent feedback. A brief survey of random lasers with incoherent feedback is presented. It is followed by a review of our recent experimental work on random lasers with coherent feedback, including measurement of the lasing threshold, lasing spectra, emission pattern, dynamical response, photon statistics, speckle pattern and the investigation of relevant length scales. Large disorder leads to spatial confinement of the lasing modes, that is the foundation for the micro random laser. Some theoretical models of random lasers with coherent feedback are briefly introduced. The study of random lasers improves our understanding of the interplay between light localization and coherent amplification.

(Some figures in this article are in colour only in the electronic version)

Contents

1. Introduction 2
2. Random laser with incoherent feedback 3
   2.1. Laser with scattering reflector 3
   2.2. Photonic bomb 4
   2.3. Powder laser 5
   2.4. Laser paint 7
3. Random laser with coherent feedback—experiment 11
   3.1. Lasing oscillation in ZnO powder 11
   3.2. Transition between two types of random laser 16
   3.3. Characteristic length scales for random laser 22
   3.4. Micro random laser 28
   3.5. A different type of random laser cavity 30

4. Random laser with coherent feedback—theory 31
4.1. Chaotic laser theory 31
4.2. Time-dependent theory 31
4.3. Analytical approach 33
4.4. Quantum theory 33
5. Interplay of light localization and coherent amplification 34
6. Applications of the random laser 35
Acknowledgments 37
References 37

1. Introduction

Both localization and laser theory were developed in the 1960s. Light scattering was traditionally considered detrimental to laser action because such scattering removes photons from the lasing mode of a conventional laser cavity. However, in a strongly scattering gain medium, light scattering plays a positive role: (i) multiple scattering increases the path length or dwell time of light in the active medium, thus enhancing light amplification by stimulated emission; (ii) recurrent light scattering provides coherent feedback for lasing oscillation. Lasing in disordered media has been a subject of intense theoretical and experimental studies. It represents the process of light amplification by stimulated emission with feedback supplied by disorder-induced scattering. There are two kinds of feedback: one is *intensity* or *energy* feedback; the other is *field* or *amplitude* feedback. The former feedback is incoherent and non-resonant, the latter is coherent and resonant. Based on the feedback mechanisms, random lasers are classified into two categories: (1) random lasers with incoherent (or non-resonant) feedback, also called incoherent random lasers, (2) random lasers with coherent (or resonant) feedback, also called coherent random lasers. This paper summarizes the research works on both types of random laser, with an emphasis on our recent experimental study of random lasers with coherent feedback.

In an amplifying random medium, light waves are multiply scattered and amplified. The relevant length scales that describe the scattering process are the scattering mean free path l_s and the transport mean free path l_t. The scattering mean free path l_s is defined as the average distance that light travels between two consecutive scattering events. The transport mean free path l_t is defined as the average distance a wave travels before its direction of propagation is randomized. These two length scales are related:

$$l_t = \frac{l_s}{1 - \langle \cos\theta \rangle}. \tag{1}$$

$\langle \cos\theta \rangle$ is the average cosine of the scattering angle, which can be found from the differential scattering cross section. Rayleigh scattering is an example of $\langle \cos\theta \rangle = 0$ or $l_t = l_s$, while Mie scattering may have $\langle \cos\theta \rangle \approx 0.5$, or $l_t \approx 2l_s$.

Light amplification by stimulated emission is described by the gain length l_g and the amplification length l_{amp}. The gain length is defined as the path length over which the intensity is amplified by a factor of e. The amplification length is defined as the (rms) average distance between the beginning and ending point for paths of length l_g. In a homogeneous medium without scattering, light travels in a straight line, thus $l_{amp} = l_g$. In the diffusive regime, $l_{amp} = \sqrt{Dt}$, where D is the diffusion coefficient, $t = l_g/v$ and v is the speed of light. In a three-dimensional (3D) system, $D = vl_t/3$, thus

$$l_{amp} = \sqrt{\frac{l_t l_g}{3}}. \tag{2}$$

The gain length is the analogue of the inelastic length defined as the travel length over which light intensity is reduced to 1/e due to absorption. Hence, the amplification length l_{amp} is analogous to the absorption length $l_{abs} = \sqrt{l_t l_i/3}$.

A random medium is characterized by its dimensionality d and size L. There are three regimes for light transport in a 3D random medium: (i) the ballistic regime, $L \leqslant l_t$; (ii) the diffusive regime, $L \gg l_t \gg \lambda$, and (iii) the localization regime, $k_e \cdot l_s \simeq 1$ (k_e is the effective wavevector in the random medium) (John 1991).

2. Random laser with incoherent feedback

2.1. Laser with scattering reflector

The two essential components of a laser are gain medium and cavity. The gain medium amplifies light through stimulated emission, and the cavity provides positive feedback. A simple laser cavity is a Fabry–Perot cavity made of two mirrors in parallel. Light returns to its original position after travelling one round trip between the mirrors. The requirement of constructive inference determines the resonant frequencies, namely

$$kL_c + \phi_1 + \phi_2 = 2\pi m, \tag{3}$$

where k is the wavevector, L_c is the cavity length, ϕ_1 and ϕ_2 represent the phases of the reflection coefficients of the two mirrors and m is an integer. Light at the resonant frequencies experiences minimum leakage loss owing to destructive interference of light leaking out of the cavity. Thus only light at the resonant frequencies spends a long time in the cavity. The long dwell time in the cavity facilitates light amplification. When the optical gain balances the loss of a resonant mode, lasing oscillation occurs in this mode. The threshold condition is (Siegman 1986)

$$R_1 R_2 \mathrm{e}^{2gL_c} = 1, \tag{4}$$

where R_1 and R_2 represent the reflectivities of the two mirrors and g is the gain coefficient of dimension 1/length.

In 1966, Ambartsumyan *et al* realized a different type of laser cavity that provides non-resonant feedback (Ambartsumyan *et al* 1966). They replaced one mirror of the Fabry–Perot cavity with a scattering surface. Light in the cavity suffers multiple scattering; its direction is changed every time it is scattered. Thus light does not return to its original position after one round trip. The spatial resonances for the electromagnetic (EM) field are absent in such a cavity. The dwell time of light is not sensitive to its frequency. The feedback in such a laser is used merely to return part of the energy or photons to the gain medium, i.e., it is energy or intensity feedback.

The non-resonant feedback can also be interpreted in terms of 'modes'. When one end mirror of a Fabry–Perot cavity is replaced by a scattering surface, escape of emission from the cavity by scattering becomes the predominant loss mechanism for all modes. Instead of individual high-Q resonances there appear a large number of low-Q resonances which spectrally overlap and form a continuous spectrum. This corresponds to the occurrence of non-resonant feedback. The absence of resonant feedback means that the cavity spectrum tends to be continuous, i.e., it does not contain discrete components at selected resonant frequencies. The only resonant element left in this kind of laser is the amplification line of the active medium. With an increase of pumping intensity, the emission spectrum narrows continuously towards the centre of the amplification line. However, the process of spectral narrowing is much slower than in ordinary lasers (Ambartsumyan *et al* 1967a). Since many modes in a laser cavity with non-resonant feedback interact with the active medium as a whole,

the statistical properties of laser emission are quite different from those of an ordinary laser. As shown by Ambartsumyan *et al* (1968), the statistical properties of the emission of a laser with non-resonant feedback are very close to those of the emission from an extremely bright 'black body' in a narrow range of the spectrum. The emission of such a laser has no spatial coherence and is not stable in phase.

Because the only resonant element in a laser with non-resonant feedback is the amplification line of the gain medium, the mean frequency of laser emission does not depend on the dimensions of the laser but is determined only by the centre frequency of the amplification line. If this frequency is sufficiently stable, the emission of this kind of laser has a stable mean frequency. Ambartsumyan *et al* (1967b) proposed using the method of non-resonant feedback to produce an optical standard for length and frequency. To realize it, they built continuous gas lasers with non-resonant feedback based on the scattering surface (Ambartsumyan *et al* 1970).

2.2. Photonic bomb

In 1968, Letokhov took one step further and proposed self-generation of light in an active medium filled with scatterers (Letokhov 1968). When the photon mean free path is much smaller than the dimension of scattering medium but much longer than the optical wavelength, the motion of photons is diffusive. Letokhov solved the diffusion equation for the photon energy density $W(\vec{r}, t)$ in the presence of a uniform and linear gain.

$$\frac{\partial W(\vec{r}, t)}{\partial t} = D\,\nabla^2 W(\vec{r}, t) + \frac{v}{l_g} W(\vec{r}, t). \tag{5}$$

v is the transport velocity of light inside the scattering medium, l_g is the gain length and D is the diffusion constant given by

$$D = \frac{v l_t}{3}. \tag{6}$$

The general solution to equation (5) can be written as

$$W(\vec{r}, t) = \sum_n a_n \Psi_n(\vec{r}) \mathrm{e}^{-(DB_n^2 - v/l_g)t}. \tag{7}$$

$\Psi_n(\vec{r})$ and B_n are the eigenfunctions and eigenvalues of the following equation:

$$\nabla^2 \Psi_n(\vec{r}) + B_n^2 \Psi_n(\vec{r}) = 0 \tag{8}$$

with the boundary condition that $\Psi_n = 0$ at a distance z_e beyond the physical boundary of the scattering medium. z_e is the extrapolation length. Usually z_e is much smaller than the dimension of scattering medium and it can be neglected. Hence, the boundary condition becomes that $\Psi_n = 0$ at the boundary of the random medium.

The solution of $W(\vec{r}, t)$ in equation (7) changes from an exponential decay to an exponential increase in time when crossing the threshold

$$DB_1^2 - \frac{v}{l_g} = 0. \tag{9}$$

B_1 is the lowest eigenvalue. If the scattering medium has the shape of a sphere of diameter L, $B_n = 2\pi n/L$, and the smallest eigenvalue $B_1 = 2\pi/L$. If the scattering medium is a cube whose side length is L, the smallest eigenvalue $B_1 = \sqrt{3}\pi/L$. Regardless of the shape of the scattering medium, the lowest eigenvalue B_1 is on the order of $1/L$. Substituting $B_1 \approx 1/L$ into equation (9), the threshold condition predicts a critical volume

$$V_{cr} \approx L^3 \approx \left(\frac{l_t l_g}{3}\right)^{3/2}. \tag{10}$$

With the fixed gain length l_g and transport mean free path l_t, once the volume of the scattering medium V exceeds the critical volume V_{cr}, $W(\vec{r}, t)$ increases exponentially with t.

This can be understood intuitively in terms of two characteristic length scales. One is the generation length L_{gen}, which represents the average distance a photon travels before generating a second photon by stimulated emission. L_{gen} can be approximated by the gain length l_g. The other is the mean path length L_{pat} that a photon travels in the scattering medium before escaping through its boundary. $L_{pat} \sim vL^2/D$. When $V \geqslant V_{cr}$, $L_{pat} \geqslant L_{gen}$. This means on average every photon generates another photon before escaping the medium. This triggers a 'chain reaction', i.e. one photon generates two photons, two photons generate four photons etc. Thus the photon number increases with time. This is the onset of photon self-generation. Because this process of photon generation is analogous to the multiplication of neutrons in an atomic bomb, this device is sometimes called a photonic bomb.

In reality the light intensity will not diverge (there is no 'explosion') because gain depletion quickly sets in and l_g increases. Taking into account gain saturation, Letokhov calculated the emission linewidth and the generation dynamics. If the scattering centres are stationary, the limiting width of the generation spectrum is determined by the spontaneous emission. Otherwise, the Brownian motion of the scattering particles leads to a random variation (wandering) of the photon frequency as a result of the Doppler effect on the scattering particles. He also predicted damped oscillation (pulsation) in the transient process of generation. Letokhov's predictions were experimentally confirmed 26 years later (Genack and Drake 1994).

2.3. Powder laser

In 1986, Markushev *et al* reported intense stimulated radiation from the $Na_5La_{1-x}Nd_x(MoO_4)_4$ powder under resonant pumping at low temperature (77 K) (Markushev *et al* 1986). When the pumping intensity exceeded a threshold, the Nd^{3+} emission spectrum was narrowed to a single line, and the emission pulse duration was shortened by approximately four orders of magnitude. Later on, they reported similar phenomena in a wide range of Nd^{3+}-activated scattering materials, including La_2O_3, La_2O_2S, $Na_5La(MoO_4)_4$, La_3NbO_7 and $SrLa_2WO_7$ (Markushev *et al* 1990). The powder was pumped by a 20 ns Q-switched laser pulse. When the pump energy reached a threshold (in the range 0.05–0.1 J cm^{-2}), a single emission pulse of 1–3 ns duration was observed. With a further increase of pump energy, the number of emission pulses increased to three or four. At a constant pumping intensity, the number of pulses, their duration and the interval between them were governed by the properties of the materials. The emission spectrum above the threshold was related to the particle shape. In a powder of shapeless particles there is only one narrow emission line at the centre of a luminescence band, while in a powder of shaped particles the emission spectrum consists of several lines in the range of the luminescence band (Ter-Garielyan *et al* 1991a). In all cases, the spectral width of the emission lines above the threshold is on the order of 0.1 nm. The observed emission was very much like laser emission. Because the particle size ($\sim$10 μm) was much larger than the emission wavelength, Markushev *et al* (1990) speculated that individual particles served as effective resonators and lasing occurred in the modes formed by total internal reflection at the surface of a particle. However, there might be some weak coupling between the neighbouring particles. In a mixture of two powders with slightly shifted luminescence bands (e.g. $Na_5La_{1-z}Nd_z(MoO_4)_4$ powders with significantly different Nd^{3+} concentrations), the emission wavelength depended on the relative concentrations of components in the mixture and the excitation wavelength (Ter-Garielyan *et al* 1991b). Briskina *et al* set up a model of

coupled microcavities to interpret the experimental result (Briskina *et al* 1996, Briskina and Li 2002). They treated the powder as an aggregate of active optically coupled microcavities and calculated the modes formed by total internal reflection (in analogue to the whispering-gallery modes). They found the quality factor of a coupled-particle cavity in the compact powder could be higher than that of a single-particle cavity due to the optical coupling. To confirm their model, they measured the spot of laser-like radiation from powders of $Al_3Nd(BO_3)_4$ and NdP_5O_{14} (Lichmanov *et al* 1998). The minimum spot size was 20–30 μm. The particle size was between 4 and 20 μm, thus the laser-like radiation was from a single particle or a few particles.

Later, a powder laser was realized with non-resonant pumping at room temperature (Gouedard *et al* 1993, Noginov *et al* 1996). The gain materials were extended from Nd^{3+}-doped powder to Ti:sapphire powder (Noginov *et al* 1998b), Pr^{3+}-doped powder (Zolin 2000) and pulverized LiF with colour centres (Noginov *et al* 1997). Although the material systems are different, the observed phenomena are similar: (i) drastic shortening of the emission pulse and spectral narrowing of the emission line above a pumping threshold; (ii) damped oscillation of the emission intensity under pulsed excitation and (iii) drifting of the stimulated emission frequency and hopping of the emission line from one discrete frequency to another within the same series of pulses. Gouedard *et al* (1993) analysed the spatial and temporal coherence of the powder laser. From the contrast of the near-field speckle pattern, they concluded that the powder emission above the threshold is spatially incoherent. This result was explained by incoherent superposition of uncorrelated speckle patterns. Their time-resolved measurement showed the speckle pattern changed rapidly in time. The estimated coherence time $\sim$ 10 psi, indicating low temporal coherence of the powder emission. Noginov *et al* (1999) also performed quantitative measurement of the longitudinal and transversal coherence with interferometric techniques. Using a Michelson (Twyman–Green) interferometer, they found the longitudinal coherence time of $Nd_{0.5}La_{0.5}Al_3(BO_3)_4$ powder (ceramics) emission was 56 ps at a pumping energy of twice the threshold. This value corresponded to 0.7 Å linewidth, in agreement with the result of direct spectroscopic linewidth measurement. They also examined the transversal spatial coherence using Young's double-slit interferometric scheme. The transversal coherence was not noticeable when the distance between two points on the emitting surface was approximately 85 μm.

Despite detailed experimental study of the powder laser, the underlying mechanism was not fully understood. Gouedard *et al* (1993) speculated that the grains of the powder emit collectively in a subnanosecond pulse with a kind of distributed feedback provided by multiple scattering. Auzel and Goldner identified two processes of coherent light generation in powder: (i) amplification of spontaneous emission by stimulated emission and (ii) synchronized spontaneous emission, namely superradiance and superfluorescence (Auzel and Goldner 2000, Zyuzin 1998, 1999). Noginov *et al* (1996) noticed the role played by photon diffusion in stimulated emission when comparing the powder laser with the single-crystal laser. The diffusive motion of light led to long path length of emission in the powder and helped to reduce the threshold. Wiersma and Lagendijk proposed a model based on light diffusion with gain (Wiersma and Lagendijk 1997a). They considered an incident pump pulse and probe pulse onto a powder slab. The active material was approximated as a four-level $(2, 1, 0', 0)$ system with the radiative transition from level 1 to $0'$ and the pumping from level 0 to 2. Fast relaxation from level 2 to 1 and from level $0'$ to 0 made both level 2 and $0'$ nearly unpopulated, thus the population of level 1 can be described by one rate equation. The whole system was described by three diffusion equations for the energy densities of the pump light $W_G(\vec{r}, t)$, the probe light $W_R(\vec{r}, t)$ and the (amplified) spontaneous emission (ASE) $W_A(\vec{r}, t)$, and one rate equation for the population density $N_1(\vec{r}, t)$ of level 1.

$$\frac{\partial W_G(\vec{r},t)}{\partial t} = D\nabla^2 W_G(\vec{r},t) - \sigma_{abs} v[N_t - N_1(\vec{r},t)]W_G(\vec{r},t) + \frac{1}{l_G} I_G(\vec{r},t), \tag{11}$$

$$\frac{\partial W_R(\vec{r},t)}{\partial t} = D\nabla^2 W_R(\vec{r},t) + \sigma_{em} v N_1(\vec{r},t) W_R(\vec{r},t) + \frac{1}{l_R} I_R(\vec{r},t), \tag{12}$$

$$\frac{\partial W_A(\vec{r},t)}{\partial t} = D\nabla^2 W_A(\vec{r},t) + \sigma_{em} v N_1(\vec{r},t) W_A(\vec{r},t) + \frac{1}{\tau_e} N_1(\vec{r},t), \tag{13}$$

$$\frac{\partial N_1(\vec{r},t)}{\partial t} = \sigma_{abs} v[N_t - N_1(\vec{r},t)]W_G(\vec{r},t) - \sigma_{em} v N_1(\vec{r},t)[W_R(\vec{r},t) + W_A(\vec{r},t)] - \frac{1}{\tau_e} N_1(\vec{r},t). \tag{14}$$

σ_{abs} and σ_{em} are the absorption and emission cross sections, τ_e is the lifetime of level 1, $I_G(\vec{r},t)$ and $I_R(\vec{r},t)$ are the intensities of the incoming pump and probe pulses, l_G and l_R are the transport mean free paths at the pump and probe frequencies and N_t is the total concentration of four-level atoms. Wiersma and Lagendijk numerically solved the above coupled nonlinear differential equations. Their simulation result reproduced the experimental observation of transient oscillation (spiking) of the emission intensity under pulsed excitation.

In the slab geometry, the critical volume predicted by Letokhov is reduced to the critical thickness $L_{cr} = \pi\sqrt{l_t l_g/3} = \pi l_{amp}$. For the fixed slab thickness L, there exists a critical amplification length $l_{cr} = L/\pi$. At the beginning of the pump pulse, the average amplification length l_{amp} decreases due to an increasing excitation level. Once l_{amp} crosses l_{cr}, the gain in the sample becomes larger than the loss through the boundaries and the system becomes unstable. This leads to a large increase of the ASE energy density. The characteristic timescale corresponding to the build-up of ASE is l_g/v. The large ASE energy density will de-excite the system again, which leads to an increase of l_{amp}. This de-excitation continues as long as the large ASE energy density is present. The characteristic timescale on which the ASE energy density diffuses out of the medium through the front or rear surface is given by L^2/D. On one hand, an overshoot of the excitation takes place because the de-excitation mechanism needs some time to set in. On the other hand, once the ASE has built up considerably, the ASE energy density can disappear only slowly due to the presence of multiple scattering, which leads to an undershoot below the threshold. These two processes result in transient oscillations of the outgoing ASE flux. The oscillations are damped because the increase of l_{amp} during the de-excitation is opposed by re-excitation owing to the presence of pump light. Therefore the system reaches the equilibrium situation $l_{amp} = l_{cr} = L/\pi$ after a few oscillations.

Both models based on light diffusion and intra-particle resonances reproduced the experimental phenomena. It is hard to tell whether the feedback in powder laser is provided by multiple scattering or total internal reflection, because the gain medium and scattering elements are not separated in the powder. Lawandy *et al* (1994) separated the scattering and amplifying media in liquid solutions. This separation allowed the scattering strength to be varied independently of the gain coefficient, and facilitated a systematic study of the scattering effect on feedback.

2.4. Laser paint

In 1994, Lawandy *et al* observed laser-like emission from a methanol solution of rhodamine 640 perchlorate dye and TiO_2 microparticles (Lawandy *et al* 1994). The dye molecules were optically excited by laser pulses and served as a gain medium. The TiO_2 particles, with a mean diameter of 250 nm, were scattering centres. The (input–output) plot of the peak emission intensity versus the pump energy exhibited a well defined pumping threshold

for the slope change. At the same threshold, the emission linewidth (full width at half maximum (FWHM)) collapsed rapidly from 70 to 4 nm, and the duration of emission pulses was shortened dramatically from 4 ns to 100 ps. The threshold behaviour suggested the existence of feedback. The relatively broad and featureless emission spectrum above the threshold indicated the feedback was frequency insensitive or non-resonant. In the solution, the feedback mechanism based on morphology-dependent resonance can be ruled out because the gain was outside the scatterer and individual scatterers were too small to serve as morphology-dependent resonators. It was found experimentally that the threshold was reduced by more than two orders of magnitude when the density of scattering particles was increased from 5×10^9 to 2.5×10^{12} cm^{-3} at the fixed dye concentration of 2.5×10^{-3} M (Sha *et al* 1994). The strong dependence of the threshold on the transport mean free path revealed that the feedback was related to scattering (Lawandy and Balachandran 1995, Zhang *et al* 1995b, Balachandran and Lawandy 1995).

However, multiple scattering or light diffusion is negligible unless the smallest dimension of the scattering medium is much larger than the transport mean free path. Experimentally when a spatially broad pump pulse was incident on a dye cell, a disc-shaped amplifying region was formed near the front window (Wiersma *et al* 1995a). The thickness of the disc was determined by the penetration depth L_{pen} of the pump light. In Lawandy's experiment, L_{pen} was close to the transport mean free path. However, the actual sample thickness (i.e., the thickness of the entire suspension) was much larger than the transport mean free path. Hence, light transport in the suspension was diffusive. Nevertheless, the emitted photons could easily escape from the thin amplifying region. Some of them escaped through the front surface into the air; the rest went deeper into the unpumped region of the suspension. After multiple scattering (or random walk), some of these photons returned to the active volume for more amplification. This return process provided energy feedback. When scattering was stronger, the return probability was higher, thus the feedback was stronger. However, incomplete feedback (less than 100% return probability) gave rise to loss. The lasing threshold was set such that the photon loss rate was balanced by the photon generation rate in the amplifying region. On one hand, the total amount of gain or amplification was the product of the amplification per unit path length and the path length travelled through the amplifying volume. The frequency dependence of the amplification per unit path length gave the highest photon generation rate at the peak of gain spectrum. On the other hand, owing to the weak frequency dependence of the transport mean free path, the feedback was nearly frequency independent within the gain spectrum; so was the loss rate for photons. Therefore, with an increase of the pumping rate, the photon generation rate in the spectral region of maximum gain first reached the photon loss rate, while outside this frequency region the photon generation rate was still below the loss rate. Then the photon density around the frequency of gain maximum built up quickly. The sudden increase of photon density near the peak of the gain spectrum resulted in an collapse of the emission linewidth.

A model based on the ring laser in the random phase limit was proposed by Balachandran and Lawandy (1997) to quantitatively explain the experimental data. The amplifying volume was approximated as a sharply bounded disc with homogeneous gain coefficient. In a Monte Carlo simulation of random walk of photons, they calculated the return probabilities R_{t1} and R_{t2} of photons to the gain volume after being launched inward and outward, and the average total path length L_{pat}. The threshold gain g_{th} is determined by the steady-state condition

$$R_{t1} R_{t2} \mathrm{e}^{g_{th} L_{pat}} = 1. \tag{15}$$

This condition is analogous to the threshold condition of a ring laser. Note that a typical ring laser has a second condition on the round-trip phase shift: $kL_{pen} = 2\pi m$, which determines the lasing frequencies. In the scattering medium the phase condition can be ignored, because the diffusive feedback is non-resonant, i.e., it requires only light return to the gain volume instead of to its original position. In fact, the probability of emitted light returning to its original position is so low in the diffusive regime that the interference effect on the feedback is negligible. Therefore this kind of laser is a random laser with non-resonant or incoherent feedback. It is also called a painted-on laser or photonic paint (Lawandy 1994, Wiersma and Lagendijk 1997b).

The discovery of Lawandy *et al* triggered many experimental and theoretical studies that can be summarized as follows.

(1) *Lasing threshold.* The dependence of lasing threshold on the dye concentration and the gain length was investigated (Zhang *et al* 1995a). Usually the threshold was reached at the point at which the pump transition was bleached. Such bleaching increased the penetration depth of the pump and consequently led to a longer path length for the emitted light within the gain region, which resulted in a reduced threshold (Siddique *et al* 1996). The influence of the excitation spot diameter on the threshold was also examined (van Soest *et al* 1999). In a suspension of TiO_2 scatterers in sulforhodamine B dye, the threshold pump intensity increased by a factor of 70 when the excitation beam diameter got close to the mean free path. This is because the large pump beam spot produced a large amplifying volume. The emitted light could travel a long path inside the active region and experienced more amplification before escaping. After the light went into the passive (unexcited) region, there was a large probability that it would return to the amplifying region because of the large pumped area. For a small excitation beam diameter, the emitted light would very likely leave the active volume after a short time, with a small chance of returning. This gave larger photon loss rate and higher threshold. The amplification by stimulated emission was found to be the strongest when the absorption length of the pump light and the transport mean free path had approximately the same magnitude (Beckering *et al* 1997). A critical transport mean free path was identified for each beam diameter, below which the threshold was almost independent of the mean free path (Totsuka *et al* 2000). These results can be explained in terms of the spatial overlap of the gain volume and the diffusion volume. By solving the coupled rate and diffusion equations, Totsuka *et al* calculated the spatial distribution of the excited state population (gain volume) and the spatial spreading of the trajectory for the luminescence light (diffusion volume). When the gain volume was smaller than the diffusion volume of the luminescence light, the amplification was not efficient as the light propagated mostly through the gainless region. If the gain volume was larger than the diffusion volume of the luminescence light, the excitation pulse energy was not used efficiently for amplification. There existed an optimized condition under which the pulse energy was used most efficiently for stimulated emission.

(2) *Emission spectra.* The stimulated emission spectrum was shifted with respect to the luminescence spectrum. This spectral shift was explained by a simple ASE model accounting for absorption and emission at the transition between the ground and first singlet excited states of the dye (Noginov *et al* 1995). Bichromatic emission was produced in a binary dye mixture in the presence of scatterers (Zhang *et al* 1995c). The dye molecules were of the donor–acceptor type, and the energy transfer between them gave double emission bands. The relative intensity of stimulated emission of the donor and the acceptor depended on the scatterer density in addition to the pumping intensity and the concentration of the dyes. The narrow-linewidth bichromatic emission was also observed in the single

dye solution with scatterers at large pumping intensity or high dye concentration (Sha *et al* 1996, Balachandran and Lawandy 1996). John and Pang (1996) explained the bichromatic emission in terms of dye molecules' singlet and triplet transitions. Using the physically reasonable estimates for the absorption and emission cross section for the singlet and triplet manifolds and the singlet–triplet intersystem crossing rate, they solved the nonlinear rate equations for the dye molecules. This leads to a diffusion equation for the light intensity in the scattering medium with a nonlinear intensity-dependent gain coefficient. Their model could account for most experimental observations, e.g. the collapse of emission linewidth at a specific threshold pump intensity, the variation of the threshold intensity with the transport mean free path, the dependence of peak emission intensity on the transport mean free path, the dye concentration and the pump intensity.

(3) *Dynamics.* One surprising result about the dynamics of stimulated emission from colloidal dye solutions is that the emission pulses can be much shorter than the pump pulses when the pumping rate is well above the threshold. For instance, 50 ps pulses of stimulated emission were obtained from the colloidal solution excited by 3 ns pulses (Sha *et al* 1994). The shortest emission pulses were $\sim$20 ps long and produced by 10 ps pump pulses (Siddique *et al* 1996). Berger *et al* (1997) modelled the dynamics of stimulated emission from random media using a Monte Carlo simulation of the random walk of pump and emitted photons. They tracked the temporal and spectral evolution of emission by following the migration of photons and molecular excitation as determined purely by local probabilities. Their simulation results revealed a sharp transition to ultrafast, narrow linewidth emission for a 10 ps incident pump pulse and a rapid approach to steady state for longer pump pulses. With a different approach van Soest *et al* (2001) also studied the dynamics of stimulated emission. They numerically solved the coupled diffusion equations for the pump light and the emitted light and the rate equation for the excited population. Their simulation result illustrated that the slow response of the population, compared to the light transport, starts a relaxation oscillation at the threshold crossing.

(4) *β factor.* Compared with the traditional laser theory, the spontaneous emission coupling factor β was introduced for the random laser (van Soest and Lagendijk 2002). In a conventional laser, β is defined as the ratio of the rate of spontaneous emission into the lasing modes to the total rate of spontaneous emission. Its value is determined by the overlap in the wavevector space between the spontaneous emission and laser field. In conventional macroscopic lasers, the spontaneous emission is isotropic while the cavity modes occupy small solid angles. The directional mismatch contributes to a small β value (less than 10^{-5}). In the scattering medium, the diffusive feedback is non-directional, thus the spatial distinction between lasing and non-lasing modes vanishes, and the only criterion is the spectral overlap of the spontaneous emission spectrum with the lasing spectrum. This gives a large β value ($\sim$0.1).

(5) *Control and optimization.* Liquid solutions are awkward to handle, e.g. the sedimentation of scattering particles in the solvent causes instability. Thus liquid solvents were replaced by polymers as host materials (Balachandran and Lawandy 1996). The polymer sheets containing laser dyes and TiO_2 nanoparticle scatterers were made with the cell-casting technique. The lasing phenomenon in solid dye solutions was similar to that in liquid dye solutions, despite the fact that the different embedding environments affect the fluorescence characteristics of the dye (Zacharakis *et al* 1999). Many techniques developed for traditional lasers were exploited to optimize and control random lasers. For example, external feedback was introduced to control the lasing threshold. de Oliveira *et al* (1997) placed a mirror close to the high-gain scattering medium, and measured the spectral line shapes of the emitted light as a function of the distance between them. The

main effect of the feedback from the mirror is to increase the lifetime of the photons inside the pump region, resulting in a reduction of the threshold pump energy. The injection-locking technique was also utilized to control the emission wavelength. Introducing a seed into the optically pumped scattering gain medium resulted in an intense isotropic emission whose wavelength and linewidth were locked to the seeding beam properties (Balachandran *et al* 1996). Moreover, multiple narrow linewidth emission was obtained by pumping one laser paint with output from another laser paint (Martorell *et al* 1996). Lately, temperature tuning has been employed to turn on and off random lasers. Liquid crystal was infiltrated into macro-porous glass, and the diffusive feedback was controlled through a change of refractive index of the liquid crystal with temperature (Wiersma and Cavalieri 2001). In a different approach, a lower critical solution temperature mixture, which could be reversibly transformed between a transparent state and a highly scattering colloid with small temperature change, was used to tune the lasing threshold with temperature (Lee and Lawandy 2002).

3. Random laser with coherent feedback—experiment

In 1998, we demonstrated a different kind of lasing process in disordered semiconductor powder and polycrystalline films (Cao *et al* 1998, 1999c). The feedback is supplied by recurrent light current. It is coherent and resonant in contrast to the diffusive feedback. Frolov *et al* also observed similar lasing phenomena in luminescent π-conjugated polymer films, organic dye-doped gel films, opal crystals saturated with polymer and laser dye solutions (Frolov *et al* 1999a, 1999b, Yoshino *et al* 1999). This kind of laser is called a random laser with coherent (or resonant) feedback.

3.1. Lasing oscillation in ZnO powder

Random lasing with coherent feedback was realized in many kinds of random medium. Although the materials are different, the phenomena are similar. In this section, the behaviour of a coherent random laser is illustrated in one of the random media used in our experiment: ZnO powder. The ZnO nanoparticles were fabricated either by physical vapour synthesis or wet chemical reaction. The particles were polydisperse with an average particle size $\sim$100 nm. The ZnO particles were either deposited onto ITO-coated substrate by electrophoresis or simply cold-pressed to form a pellet. The sample thickness varied from 10 μm to 1 mm. The filling factor is around 50%.

The transport mean free path l_t was characterized in a coherent backscattering (CBS) experiment (Kuga and Ishimaru 1984, van Albada and Lagendijk 1985, Wolf and Maret 1985). ZnO has a direct bandgap of 3.3 eV. Strong absorption makes it very difficult to measure l_t at photon energy equal to or above the bandgap. To avoid absorption, the probe photon energy was set at 3.0 eV. The probe beam was the second harmonic ($\lambda = 410$ nm) of a mode-locked Ti:sapphire laser (76 MHz repetition rate, 200 fs pulse width). The angular width (FWHM) $\Delta\theta$ of the backscattering cone is determined by the transport mean free path l_t:

$$\Delta\theta \simeq \frac{0.7 n_e (1 - R)}{k_e l_t}, \tag{16}$$

where n_e is the effective refractive index of the ZnO powder sample, k_e is the effective wavevector of the probe light in the sample and R is the diffusive reflectivity of the sample–air interface. From $\Delta\theta$, we estimated $l_t \sim \lambda$. Such short transport mean free path indicated very strong optical scattering in the ZnO powder. Note that the probe frequency was lower than the

ZnO emission frequency. l_t for the emitted light should be shorter than the measured value, because the refractive index of ZnO increases as the photon energy approaches the bandgap.

The ZnO samples were optically excited by the third harmonic ($\lambda = 355$ nm) or the fourth harmonic ($\lambda = 266$ nm) of a pulsed Nd:YAG laser (10 Hz repetition rate, 20 ps pulse width). The pump beam was focused to a spot or a stripe on the sample surface. Electrons in the ZnO valence band absorbed pump photons and jumped to the conduction band. They subsequently relaxed to the bottom of the conduction band before radiative decay. The spectrum of ZnO emission was measured by a 0.5 m spectrometer with a liquid-nitrogen-cooled CCD array detector. The spectral resolution was about 1.3 Å. Simultaneously, the spatial distribution of the emitted light intensity at the sample surface was imaged by an ultraviolet (UV) microscope onto a UV sensitive CCD camera. The amplification of the microscope was about 100 times. The spatial resolution was $\sim$0.3 μm. A bandpass filter was placed in front of the microscope objective lens to block the pump light.

Figure 1 shows the evolution of the emission spectra with the pump intensity. At low excitation intensity, the spectrum consisted of a single broad spontaneous emission peak. As the pump power increased, the emission peak became narrower owing to preferential amplification at frequencies close to the maximum of the gain spectrum. When the excitation intensity exceeded a threshold, discrete narrow peaks emerged in the emission spectra. The linewidth of these peaks was less than 2 Å, which was less than 1/30 of the linewidth of the ASE peak below the threshold. When the pump intensity increased further, more sharp peaks appeared. The frequencies of the sharp peaks depended on the sample position. As we moved the excitation spot across the sample, the frequencies of the sharp peaks changed. This phenomenon suggests that the discrete spectral peaks result from spatial resonances for light in the ZnO powder, and such resonances are related to the local configurations of ZnO particles. Since individual ZnO nanoparticles are too small to serve as morphology-dependent resonators, the possibility of intra-particle resonances formed by total internal reflection at particle surface can be ruled out. Thus the origin of the spatial resonances lies in the inter-particle scattering. Due to very strong scattering, recurrent light scattering events arise, i.e., after multiple scattering light returns to a scatterer from which it has been scattered before. The interference of the return light is constructive only at certain frequencies. Therefore, the requirement for constructive interference of backscattered light selects the resonant frequencies.

Figure 2 is a plot of the integrated emission intensity versus the excitation intensity. A threshold behaviour was observed: above the pump intensity at which discrete spectral peaks emerged, the emission intensity increased much more rapidly with the excitation intensity. Figure 3 exhibits the emission patterns below and above the threshold. Below the threshold, the spatial distribution of the spontaneous emission intensity was smooth across the excitation area. Due to the pump intensity variation across the excitation spot, the spontaneous emission in the centre of the excitation spot was stronger. Above the threshold, as soon as the discrete spectral peaks emerged, spatially separated regions of intense radiation appeared in the image of the emitted light distribution on the sample surface. Each region consisted of a few bright spots whose size was between 0.3 and 0.6 μm. This phenomenon can be explained as follows: due to local variation of particle density and spatial distribution, there exist small regions of stronger scattering. Light can be trapped in these regions through multiple scattering and interference. For a particular configuration of ZnO nanoparticles, only light at certain frequencies can be confined, because the interference effect is frequency sensitive. In a different region of the sample, the particle configuration is different, thus light at different frequencies is confined. In other words, there are many resonant cavities formed by recurrent scattering and interference. Incomplete trapping of light gives rise to cavity loss. When the optical gain reaches the cavity loss, laser oscillation occurs in the cavity modes, that gives discrete lasing peaks in the emission

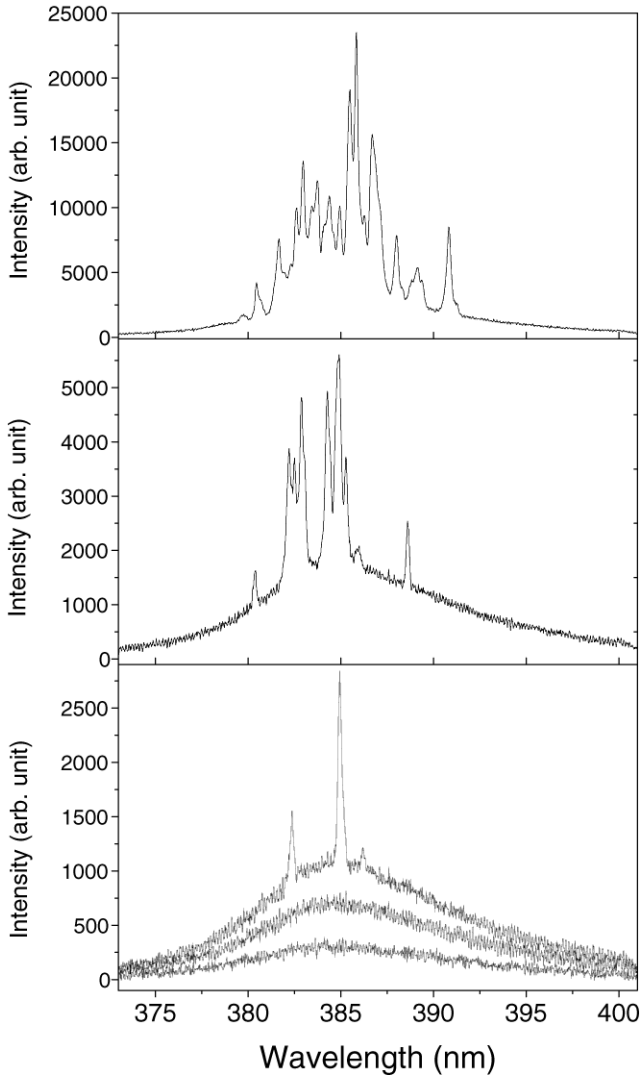

Figure 1. Spectra of emission from ZnO powder when the excitation intensity is (from bottom to top) 400, 562, 763, 875 and 1387 kW cm^{-2}.

spectrum (figure 1). Due to the presence of a large number of defects in the ZnO particles, non-radiative recombination of the excited carriers is significant below the lasing threshold. Above the lasing threshold, the fast stimulated emission process makes the radiative recombination of the excited carriers dominate over the non-radiative recombination. This results in a rapid increase of emission intensity (figure 2).

The temporal evolution of emission was measured by a streak camera (Soukoulis *et al* 2002). The temporal resolution is 2 ps. Figure 4 shows the time traces of emission below the threshold (a), just above the threshold (b) and well above the threshold (c). Below the threshold, the decay time of the emission was 167 ps. When the pump intensity exceeded the threshold, the emission pulse was shortened dramatically. The initial decay of emission intensity was very fast. The decay time was 27 ps. After $\sim$50 ps, the fast decay was replaced

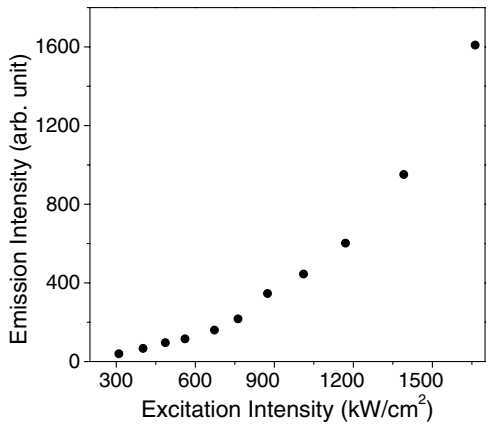

Figure 2. The integrated intensity of emission from the ZnO powder versus the excitation intensity.

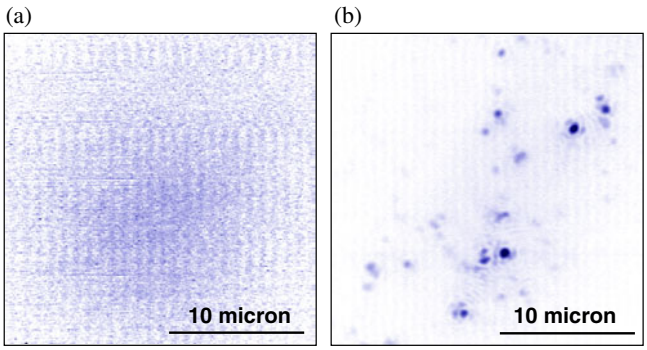

Figure 3. The spatial distribution of emission intensity in ZnO powder. The incident pump pulse energy is 5.2 nJ for (a) and 12.5 nJ for (b).

by a slow decay. The later decay time was 167 ps, which was equal to the decay time below the threshold. The initial fast decay was caused by rapid stimulated emission, and the later slow decay resulted from spontaneous emission and non-radiative recombination. As the pump intensity was increased further, the initial stimulated emission became much stronger than the later spontaneous emission. The drastic shortening of the emission pulses provides additional evidence for lasing in the ZnO powder. Next we investigated the dynamics of individual lasing modes. The emission from the sample was directed to the entrance slit of a 0.5 m spectrometer. The output port of the spectrometer was connected to the streak camera whose entrance slit was perpendicular to that of the spectrometer. By combining the spectrometer with the streak camera, we were able to separate different lasing modes and obtain the time trace of each lasing mode. Figure 5 is a spectral–temporal image taken by the streak camera. The horizontal axis is the time, and the vertical axis is the wavelength. We noticed that lasing in different modes was turned on and off at different times. The unsynchronized temporal behaviours of these lasing modes suggest that they originate from different cavities that have different quality factors. When the pump intensity was near the lasing threshold, relaxation oscillation was observed for some of the lasing modes. The oscillation period varied from mode to mode. This again indicates that the lasing modes are from different cavities with different photon lifetimes.

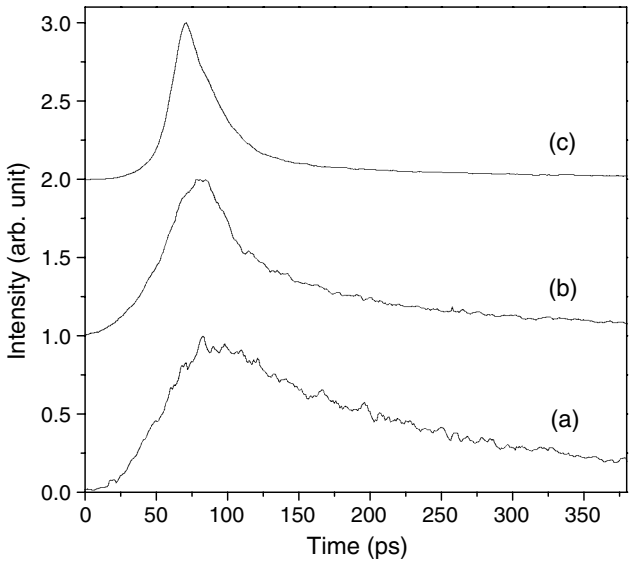

Figure 4. The temporal evolution of the emission intensity from ZnO powder below the lasing threshold (a), just above the lasing threshold (b) and well above the lasing threshold (c). The curves are shifted vertically for clarity; the maximum intensity of each curve is normalized to unity.

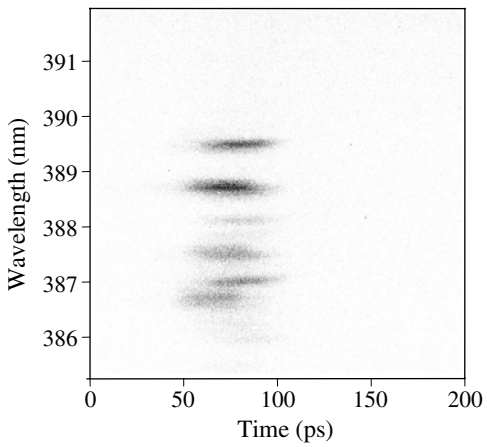

Figure 5. The spectral–temporal image of ZnO emission taken by the streak camera. The incident pump pulse energy is 4.5 nJ.

Finally the quantum statistical property of laser emission from the ZnO powder was probed with the spectrometer–streak camera set-up (Cao *et al* 2001). The streak camera operated in the photon counting mode. To measure the photon statistics of a single lasing mode, we drew a box around the centre of an emission peak on the spectral–temporal image (figure 5). One side of the box corresponds to the wavelength interval $\Delta\lambda = 0.12$ nm; the other side is the time interval $\Delta t = 3.9$ ps. The number of photons inside this box was counted for each pulse. After collecting photon count data for a large number of pulses, the probability $P(n)$ of n photons within the wavelength interval $\Delta\lambda$ and the time interval Δt was obtained. Because the sampled radiation field was within a frequency interval $\Delta\nu \simeq c\Delta\lambda/\lambda^2$, its relaxation must

occur on the timescale longer than $1/\Delta\nu$. We set the sampling time $\Delta t < 1/\Delta\nu$ so that it was shorter than the coherence time of the radiation field. From another point of view, because $\Delta\nu \cdot \Delta t = 0.95 < 1$, the counting area corresponded to a single EM mode. For single-mode coherent light, the photon number distribution $P(n)$ satisfies the Poisson distribution

$$P(n) = \frac{\langle n\rangle^n \mathrm{e}^{-\langle n\rangle}}{n!} \tag{17}$$

where $\langle n\rangle$ is the average photon number. For single-mode chaotic light, the photon number distribution $P(n)$ satisfies the Bose–Einstein (B–E) distribution

$$P(n) = \frac{\langle n\rangle^n}{[1+\langle n\rangle]^{n+1}}. \tag{18}$$

Note that the above distribution holds only for a single mode. For multimode chaotic light, the photon number distribution approaches the Poisson distribution. From the measured $P(n)$, we obtained the normalized second-order correlation coefficient G_2

$$G_2 = 1 + \frac{\langle(\Delta n)^2\rangle - \langle n\rangle}{\langle n\rangle^2}. \tag{19}$$

For the Poisson distribution, $G_2 = 1$. For the B–E distribution, $G_2 = 2$.

Figure 6(a) shows the measured $P(n)$ of ZnO emission at the threshold where discrete spectral peaks appear. The measured photon count distribution was almost identical to the B–E distribution of the same count mean. The value of G_2 was 1.94. As we increased the pump intensity, the photon statistics of ZnO emission started deviating from the B–E statistics. As shown in figure 6(b), when the pump intensity was 1.5 times the threshold, the measured photon count distribution was between the B–E distribution and the Poisson distribution. G_2 became 1.51. When the pump intensity increased to three times the threshold, the photon count distribution of ZnO emission got closer to the Poisson distribution (figure 6(c)). G_2 reduced to 1.19. Eventually, when the pump intensity was 5.6 times the threshold, the photon count distribution was nearly identical to the Poisson distribution (figure 6(d)). The corresponding G_2 was 1.06. Figure 7 is a plot of the second-order correlation coefficient G_2 versus the pump intensity. As the pump intensity increased, G_2 decreased gradually from two to unity. Because we took only a finite number of pulses in the measurement, the rms error in G_2 was equal to $(2/K\langle n\rangle^2)^{1/2}$, where K was the number of pulses. The sampling error for G_2 was calculated and plotted for each data point in figure 7. Figures 6 and 7 illustrate that the photon statistics of the emitted light from the ZnO powder changes continuously from B–E statistics at the threshold to Poisson statistics well above the threshold.

The photon statistics of the random laser with coherent feedback is similar to that of a traditional laser, but very different from the photon statistics of the random laser with incoherent feedback (Zacharakis *et al* 2000). In a random laser with coherent feedback, the photon number fluctuation in each mode is quenched by gain saturation well above the threshold. For a random laser with incoherent feedback, only the fluctuation of the total number of photons in all modes of laser emission is suppressed by gain saturation, while the photon number fluctuation in a single mode is not affected. This difference will be explained in the next section.

3.2. Transition between two types of random laser

The previous section illustrates that the behaviour of the random laser with coherent feedback is quite different from that of the random laser with incoherent feedback. To understand their difference, we studied the transition between them by varying the amount of scattering in the gain medium (Cao *et al* 2000a). The random media used in this experiment are

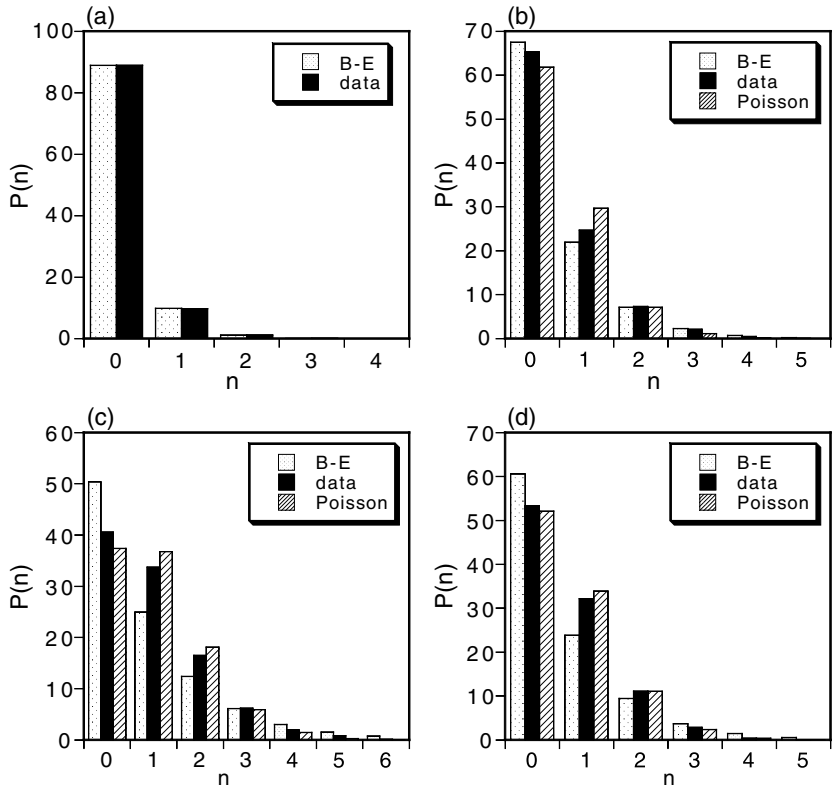

Figure 6. The solid columns are the measured photon count distribution of the emission from the ZnO powder. The dotted (dashed) columns are the B–E (Poisson) distribution for the same count mean. The incident pump intensity is (a) 1.0, (b) 1.5, (c) 3.0, (d) 5.6 times the threshold intensity where discrete spectral peaks appear.

rhodamine 640 dye solutions containing ZnO nanoparticles. The advantage of the solutions is that the scattering length can be varied continuously through the change of particle density in the solutions.

The frequency-doubled output ($\lambda = 532$ nm) of a pulsed Nd:YAG laser (10 Hz repetition rate, 20 ps pulse width) was used to excite the dye molecules in the solution. The emission spectrum was captured after a single pump pulse. Figure 8 shows the evolution of the emission spectra with the pump intensity when the particle density was $\sim 2.5 \times 10^{11}$ cm^{-3}. The dye concentration was fixed at 5×10^{-3} M. When the pump intensity crossed a threshold, a drastic spectral narrowing occurred. As shown in the insets of figure 8, once above the threshold, the emission linewidth collapsed to $\sim$5 nm. Simultaneously, the peak emission intensity increased dramatically. This phenomenon was identical to what Lawandy *et al* (1994) had observed. It corresponded to lasing with non-resonant feedback occurring in the colloid.

Next the ZnO particle density was increased to 5×10^{11} cm^{-3} while the dye concentration was kept constant. Figure 9 reveals two thresholds. As the pump intensity increased, it reached the first threshold where the emission spectrum quickly narrowed to about 5 nm. As the pump intensity increased further, it reached the second threshold where discrete spectral peaks of linewidth less than 0.2 nm emerged. The phenomenon above the second lasing threshold was similar to that in the ZnO powder. It corresponded to lasing with coherent feedback. Because

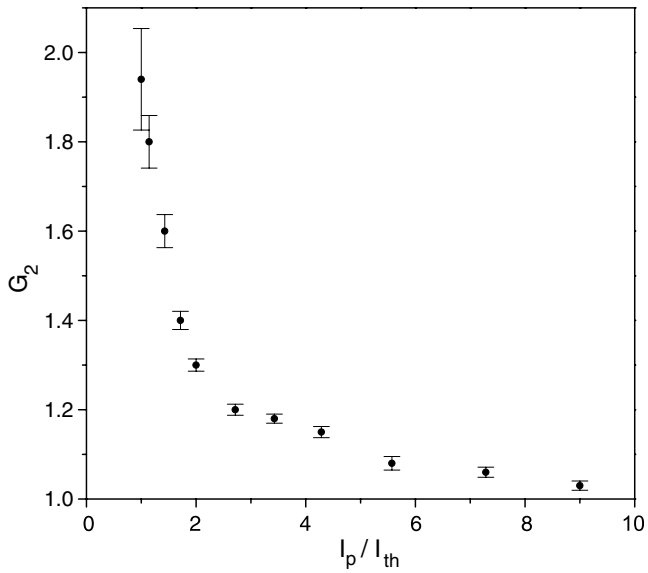

Figure 7. The second-order correlation coefficient G_2 as a function of the ratio of the incident pump intensity I_p to the threshold intensity I_{th}.

the ZnO particles were mobile in the solution, the random cavities constantly changed their configurations. Thus the frequencies of the lasing modes are different for each pump pulse. The spectra shown in figures 8–10 were taken after single pump pulse.

Finally, the ZnO particle density was increased to 1×10^{12} cm^{-3}. As shown in figure 10, with an increase of the pump intensity, the discrete spectral peaks appeared before the collapse of the emission linewidth. This indicates the threshold for lasing with coherent feedback become lower than the threshold for lasing with incoherent feedback in the strong scattering medium.

The above phenomena can be understood in terms of the eigenmodes of the Maxwell equations in a random medium. Owing to the finite size of the random medium, the eigenenergies are complex numbers, whose imaginary parts represent the decay rates. Through the coupling to the outside reservoir (i.e., to the EM modes outside the random medium), the eigenmodes interact with each other. Photons can hop from one mode to another through scattering at the boundary. In the delocalization regime, the average decay rate of an eigenmode is larger than the mean frequency spacing of adjacent modes. Hence, the eigenmodes are spectrally overlapped, giving a continuous emission spectrum. When scattering is weak, the eigenmodes are strongly coupled. Due to photon exchange among the modes, the photon loss rate for a set of interacting modes is much lower than that for a single mode. In an active random medium, when the optical gain for a set of interacting modes at the frequency of gain maximum reaches the loss of these coupled modes, the total photon number in these coupled modes builds up. This process is lasing with incoherent (or non-resonant) feedback. The quick increase of photon number at the frequency of gain maximum results in sudden spectral narrowing (figure 8). Well above the threshold, gain saturation quenches the total photon number fluctuation. However, strong coupling of the eigenmodes (e.g., photon hopping among the modes) prevents stabilization of the photon number in a single mode.

With an increase in the amount of optical scattering, the dwell time of light in the random medium increases. The decrease of their coupling to the outside reservoir weakens the

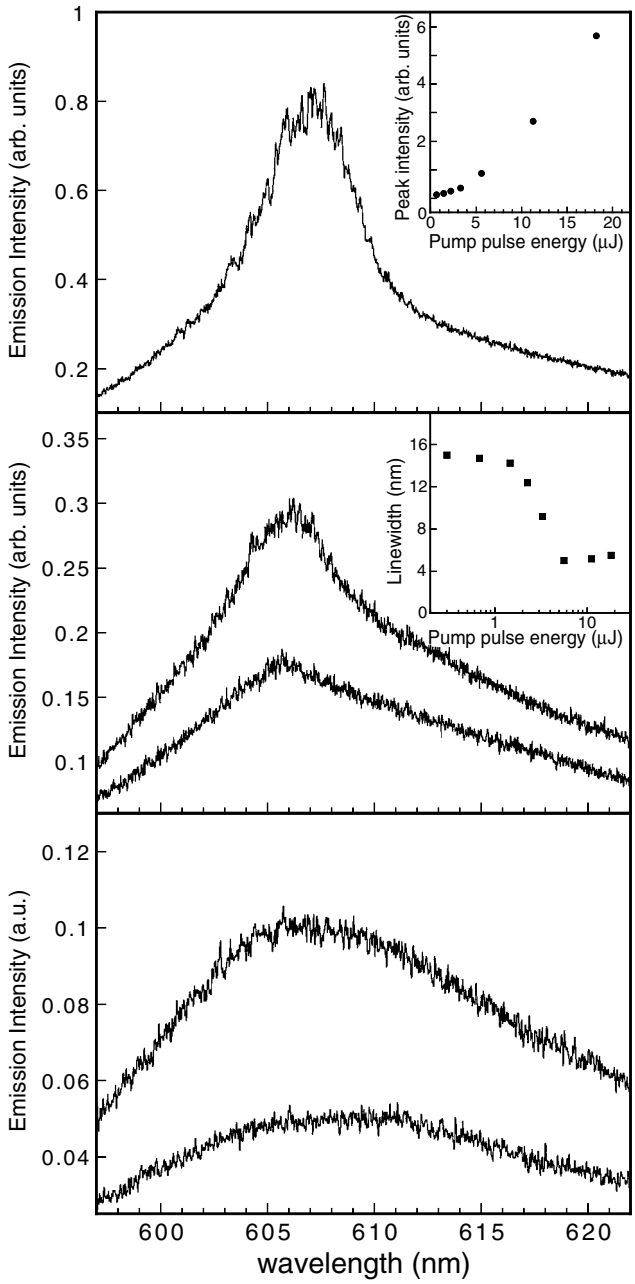

Figure 8. Spectra of emission from the rhodamine 640 dye solution containing ZnO nanoparticles. The ZnO particle density is $\sim 3\times 10^{11}$ cm^{-3}. The incident pump pulse energy is (from bottom to top) 0.68, 1.5, 2.3, 3.3, 5.6 μJ. The upper inset is the emission intensity at the peak wavelength versus the pump pulse energy. The middle inset is the emission linewidth versus the pump pulse energy.

interaction among the modes. When the optical gain increases, it first reaches the threshold for lasing in a set of coupled modes at the frequency of gain maximum. As the optical gain increases further, it reaches the loss of a single mode with long lifetime. Then, lasing occurs in

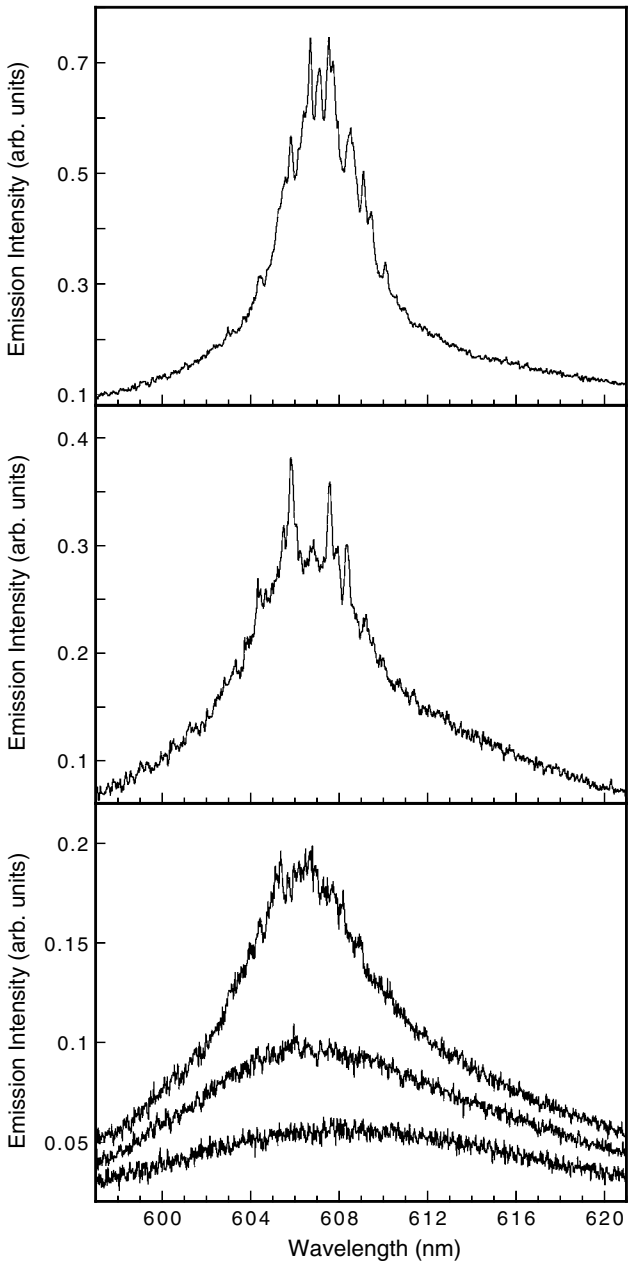

Figure 9. Spectra of emission from the rhodamine 640 dye solution containing ZnO nanoparticles. The ZnO particle density is $\sim 6 \times 10^{11}$ cm^{-3}. The incident pump pulse energy is (from bottom to top) 0.74, 1.35, 1.7, 2.25 and 3.4 μJ.

a this mode. A further increase of optical gain leads to lasing in more low-loss modes. Laser emission from these modes gives discrete peaks in the emission spectrum (figure 9).

When the scattering strength increases further, the decay rates of the eigenmodes and the coupling among them continue decreasing. There are a small number of eigenmodes with extremely long lifetime and nearly decoupled from other modes. The threshold gain for lasing

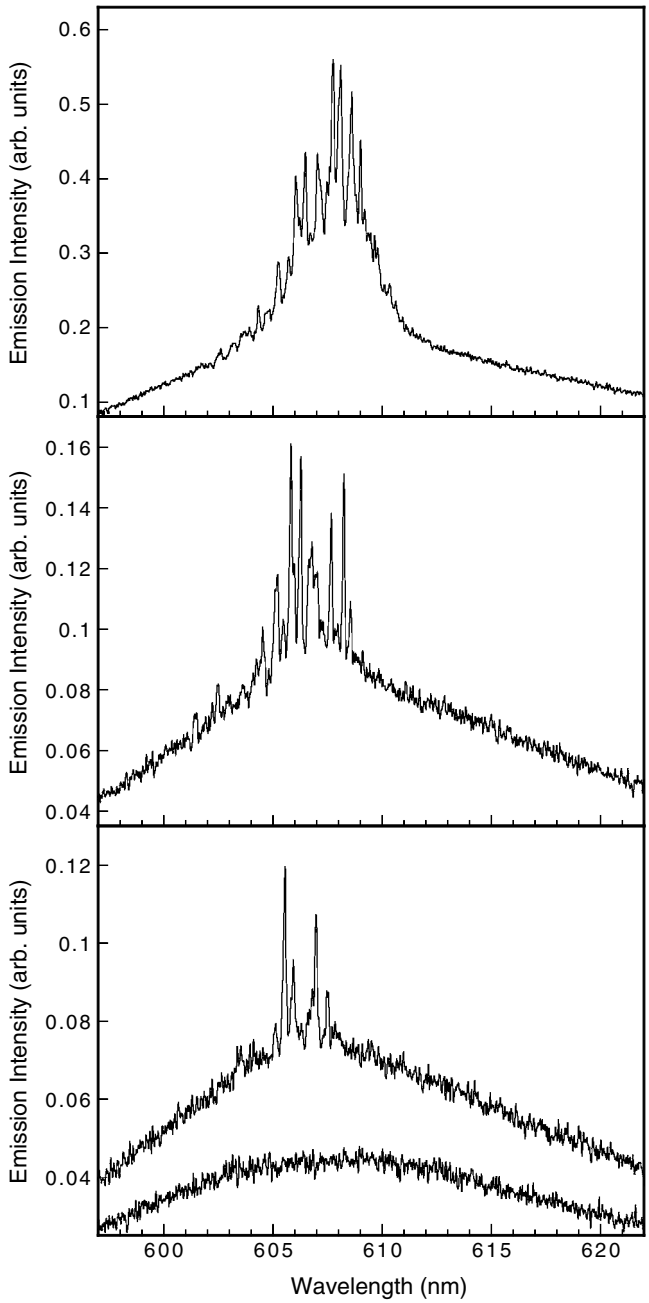

Figure 10. Spectra of emission from the rhodamine 640 dye solution containing ZnO nanoparticles. The ZnO particle density is $\sim 1 \times 10^{12}$ cm^{-3}. The incident pump pulse energy is (from bottom to top) 0.68, 1.1, 1.3 and 2.9 μJ.

in these individual modes becomes lower than the threshold gain for lasing in a set of coupled modes. Then lasing with coherent feedback occurs first (figure 10). Because of weak coupling of the lasing modes, the photon number fluctuation in each mode is quenched by the gain saturation effect well above the threshold.

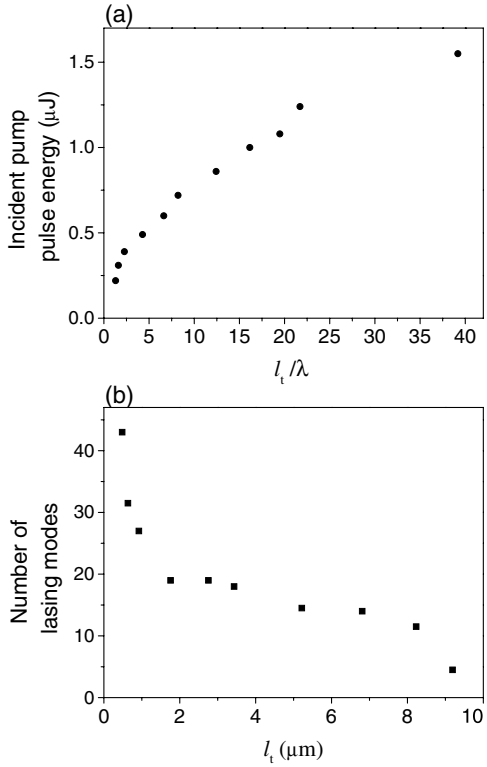

Figure 11. (a) The incident pump pulse energy at the lasing threshold versus l_t/λ. (b) The number of lasing modes as a function of l_t at the fixed incident pump pulse energy of 1.0 μJ.

3.3. Characteristic length scales for random laser

Despite different feedback mechanisms, the relevant length scales for the coherent random laser are the same as those for the incoherent random laser: the transport mean free path, the gain length, the size of the random medium and the gain volume. A detailed study on the dependence of the lasing threshold and the number of lasing modes on these length scales can be found in (Ling *et al* 2001).

The random media used in this study were PMMA sheets containing rhodamine 640 perchlorate dye and TiO_2 particles. The sample thickness was between 200 and 500 μm. The mean diameter of TiO_2 particles was 400 nm. The TiO_2 particle density in PMMA was varied from 8×10^{10} to 6×10^{12} cm^{-3}. The transport mean free path was characterized in the CBS experiment. The output from a He:Ne laser was used as the probe light, since its wavelength was very close to the emission wavelength of rhodamine 640 perchlorate dye. To avoid absorption of the probe light, the PMMA samples used in the CBS experiment contained only nanoparticles and not dye.

The PMMA sheets containing dye and nanoparticles were optically excited by the second harmonic of a pulsed Nd:YAG laser. The pump beam was focused to a spot of 50 μm on the sample surface. Figure 11(a) is a plot of the incident pump pulse energy at the lasing threshold versus the transport mean free path. The dye concentration was fixed at 5×10^{-2} M. As the TiO_2 particle density in the PMMA sheet increases, the transport mean free path decreases, and the lasing threshold also decreases. The strong dependence of the lasing threshold on

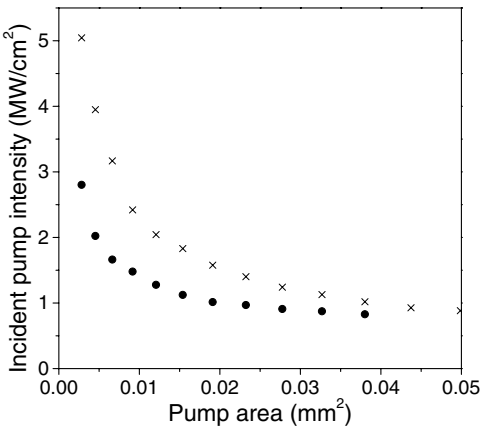

Figure 12. The incident pump intensity at the lasing threshold versus the area of the pump beam spot on the sample surface. l_t are 0.9 μm (circles), and 9 μm (crosses), respectively.

the transport mean free path confirms the important contribution of scattering to lasing. With an increase in the amount of optical scattering, the feedback provided by scattering becomes stronger. In other words, the resonant cavities formed by recurrent light scattering have lower loss. Hence, the lasing threshold is reduced. Figure 11(b) shows the number of lasing modes in the samples with different transport mean free paths at the same pump intensity. The shorter the transport mean free path is, the more lasing modes emerge. This is because, in a sample of stronger scattering, there are more low-loss cavities formed by recurrent scattering. At a fixed optical gain, in more cavities the loss is balanced by gain, and lasing oscillation occurs. One surprise in figure 11(a) is that lasing with resonant feedback occurs in samples of $l_t \gg \lambda$. Despite the fact that the coherent feedback provided by scattering is rather weak (in other words, the cavities formed by recurrent scattering are lossy), lasing can still occur as long as the dye concentration and the pump intensity are high enough. Another interesting feature in figure 11 is that when the transport mean free path approaches the optical wavelength, the lasing threshold pump intensity drops quickly, and the number of lasing modes increases dramatically. This result agrees with the prediction by John and Pang of a dramatic threshold reduction in the regime $l_t \to \lambda$ of incipient photon localization (John and Pang 1996).

The lasing threshold also depends on the pump area. The PMMA sheet was initially placed at the focal plane of a lens. Then the lens was moved away from the sample to increase the size of the pump beam spot on the sample. The incident pump intensity I_{th} at the lasing threshold was recorded as a function of the area A of the pump spot on the sample surface. Figure 12 shows the data for two samples with l_t of 0.9 and 9 μm. As the pump area increased, the lasing threshold first decreased then saturated. There existed a critical pump area above which the lasing threshold was nearly independent of the pump area. The shorter the transport mean free path, the smaller the critical area. In order to understand this result, we need to find out how big the lasing modes are. Unfortunately, it is impossible to measure the distribution of the laser field inside the random medium. Owing to the short penetration length of the pump light, optical gain is confined to a region next to the sample surface. Only the modes located close to the sample surface have spatial overlap with the gain volume and experience amplification. Therefore, the lasing modes are located close to the sample surface, and we can probe the spatial distribution of the lasing modes at the sample surface.

We developed a spectrally resolved speckle technique to map the spatial profile of individual lasing modes at the sample surface (Cao *et al* 2002). Previous speckle measurement

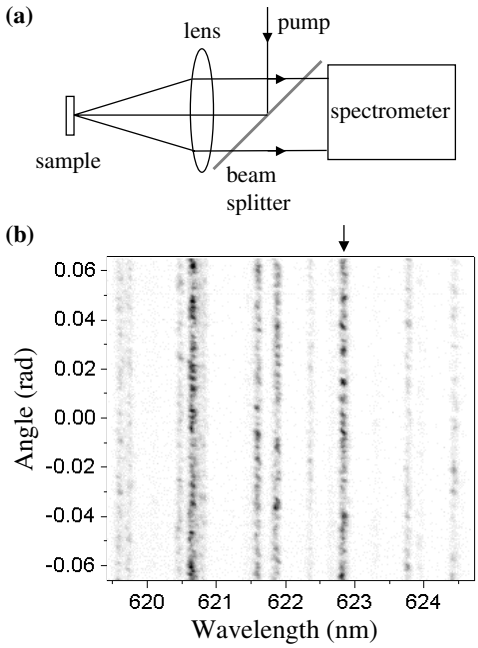

Figure 13. (a) Schematic experimental geometry for the spectrally resolved speckle measurement of laser emission from the random medium. (b) Part of a spectral image of the emission from the polymer containing dye and microparticles. The incident pump pulse energy is 0.98 μJ.

revealed an increase of path length of an external probe light travelling in an amplifying random medium (van Soest *et al* 2002). We measured the speckle of coherent laser emission from the random medium. The experimental geometry is shown schematically in figure 13(a). The pump beam was focused by a lens (5 cm focal length) onto the polymer sheet at normal incidence. The pump spot at the sample surface is about 50 μm in diameter. The emission from the sample was collected by the same lens and directed to a 0.5 m spectrometer with a cooled CCD array detector. The distance from the lens to the spectrometer's entrance slit was nearly equal to the focal length of the lens. Because the polymer sheet was placed at the focal plane of the lens, the emission from the polymer sheet was collimated before entering the spectrometer. The spectrometer imaged its entrance slit onto the two-dimensional (2D) CCD array detector with 1:1 ratio.

Figure 13(b) is part of a spectral image taken by the CCD array detector above the lasing threshold. The horizontal axis is the wavelength, and the vertical axis is the angle. Below the lasing threshold, the emission spectrum had a single broad spontaneous emission peak. The spontaneous emission intensity was invariant with the angle. Above the threshold, discrete lasing peaks emerged in the emission spectrum. For each spectral peak, the emission intensity fluctuated randomly with the angle. The emergence of speckle is a direct evidence of coherent emission from the sample. As shown in figure 13(b), different spectral peaks exhibited different speckle patterns. When the pump intensity was increased further, the contrast of speckle pattern, i.e., the amplitude of intensity variation, increased as the emission became more coherent.

The far-field speckle pattern of a lasing state is determined by its field pattern at the sample surface. The angular distribution of the outgoing field $E(q)$ is the Fourier transform of the

field pattern $E(x)$ at the surface,

$$E(q) = \int E(x) e^{i2\pi qx} dx, \tag{20}$$

where $q \equiv \sin\theta/\lambda$, θ is the angle between the emission direction and the normal of the sample-air interface and x represents the transverse coordinate at the sample surface. The angular distribution of the emission intensity $I(q) \equiv |E(q)|^2$ can be obtained experimentally from the far-field speckle pattern. The spatial field correlation function at the sample surface $C_E(x) \equiv \int E^*(x')E(x+x')\,dx'$. According to equation (20), $C_E(x)$ and $I(q)$ form a Fourier transform pair, namely,

$$C_E(x) = \int I(q) e^{-i2\pi xq}\, dq. \tag{21}$$

Therefore, the speckle pattern of a lasing state gives its spatial field correlation function.

From the 2D spectral image in figure 13(b), we obtained the angular dependence $I(q)$ of the emission intensity for the lasing peak at $\lambda = 622.8$ nm (marked by an arrow). $I(q)$ was normalized: $\langle I(q)\rangle = 1$. The discrete Fourier transform of $I(q)$ gave the spatial field correlation function, whose amplitude is plotted in figure 14(a). The spatial resolution δx for $C_E(x)$ is determined by the angular range Δq of $I(q)$, i.e., $\delta x = 1/\Delta q$. Because the diameter of the lens is larger than the width of the CCD array detector, the maximum collecting angle for the emission $\theta_m = \arctan(D/2f) = 0.066$, where $f = 50$ mm is the focal length of the lens and $D = 6.6$ mm is the width of the CCD array detector. Since $\theta_m \ll 1$, $\sin\theta \approx \theta$, and $q \approx \theta/\lambda$. $\Delta q \approx 2\theta_m/\lambda \approx D/f\lambda \approx 0.21\ \mu\text{m}^{-1}$. $\delta x \approx 4.7\ \mu$m. The spatial range Δx for $C_E(x)$ is determined by the angular resolution δq, i.e., $\Delta x = 1/\delta q$. Because the emitted light is collimated by the lens, the angular resolution depends on the size s of each CCD pixel. $s = 26\ \mu$m. $\delta q \approx s/f\lambda = 0.832\ \text{mm}^{-1}$. $\Delta x \approx 1.2$ mm. As a result of Fourier transform in the finite range of q, the value of $C_E(0)$ is inaccurate and should be discarded.

As shown in figure 14(a), the profile of $|C_E(x)|$ has some peaks and valleys. It reflects the field pattern $E(x)$. The integration of $|C_E(x)|$ gives

$$S(x) \equiv \int_x^\infty |C_E(x')|\,dx' \simeq \int_x^{\Delta x/2} |C_E(x')|\,dx'. \tag{22}$$

Experimentally $|C_E(x)|$ falls to nearly zero when x approaches $\Delta x/2$. Hence, we replaced ∞ by $\Delta x/2$ for the upper limit of the integral in equation (22). Figure 14(b) is a plot of $S(x)$ obtained by integrating $|C_E(x)|$ in figure 14(a). $S(x)$ is a smoother function of x than $|C_E(x)|$. The dotted curve in figure 14(b) represents the fit of $S(x)$ with an exponential decay function, $S(x) = A_0 \exp(-x/l_d)$, where A_0 and l_d are the fitting parameters. $S(x)$ fit very well with the exponential decay function, the chi squared $\chi^2 = 0.0026$. The decay length $l_d = 131.8\ \mu$m. We also fitted $S(x)$ with an algebraic decay function $S(x) = c_1/x^{c_2}$, where c_1 and c_2 are the fitting parameters. The fit was very bad, $\chi^2 = 0.46$. The above speckle analysis was applied to other lasing peaks in figure 13(b). Their spatial field correlation functions were different. Nevertheless, $S(x)$ always fitted well with an exponential decay function, but not an algebraic decay function. The decay length varied from peak to peak. The exponential decay of $S(x)$ suggests that the envelope of the spatial field correlation function falls exponentially with x; namely, $|C_E(x)| \sim \exp(-x/l_d)$.

We measured the spatial field correlation functions over a wide range of pump intensity, from the threshold where discrete spectral peaks appear to well above the threshold. Figure 15(a) is a plot of the decay length l_d versus the pump intensity for one lasing mode. The pump intensity I_p was normalized to the threshold value I_{th} where this lasing peak just

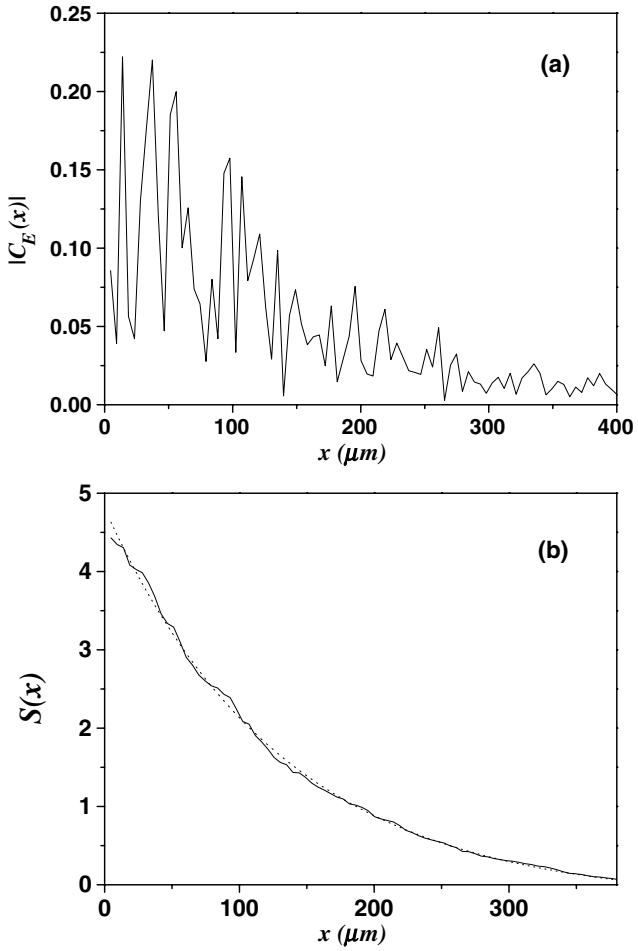

Figure 14. (a) The amplitude of the spatial field correlation function $|C_E(x)|$ for the lasing peak at $\lambda = 622.8$ nm in figure 13(b) (marked by an arrow). (b) The solid curve is $S(x)$ obtained by integrating $|C_E(x)|$ in (a). The dotted curve represents the fit with an exponential decay function.

emerged in the emission spectrum. $S(x)$ was fitted with an exponential decay function. The fitting error χ^2 is plotted in figure 15(b). Just above the threshold, the exponential fit of $S(x)$ was not good, as indicated by the relatively large value of χ^2. The decay length $l_d = 365$ μm. With an increase of the pump intensity, χ^2 decreased, suggesting the exponential fit became better. The decay length also decreased. Eventually, $S(x)$ fitted very well with an exponential decay. The decay length did not change with the pump intensity any longer. The behaviour of the decay length can be explained as follows. When the lasing peak just appears in the emission spectrum, its intensity is lower than the ASE intensity. The large decay length indicates the ASE is spread over a large region. As the pump intensity increases, the emission intensity of the lasing state increases more rapidly than the ASE intensity. When the emission intensity of the lasing state becomes much higher than the ASE intensity, the wavefunction of the lasing state dominates the spatial field correlation function. The independence of the decay length from the pump intensity suggests the wavefunction of the lasing mode does not change with the pumping rate.

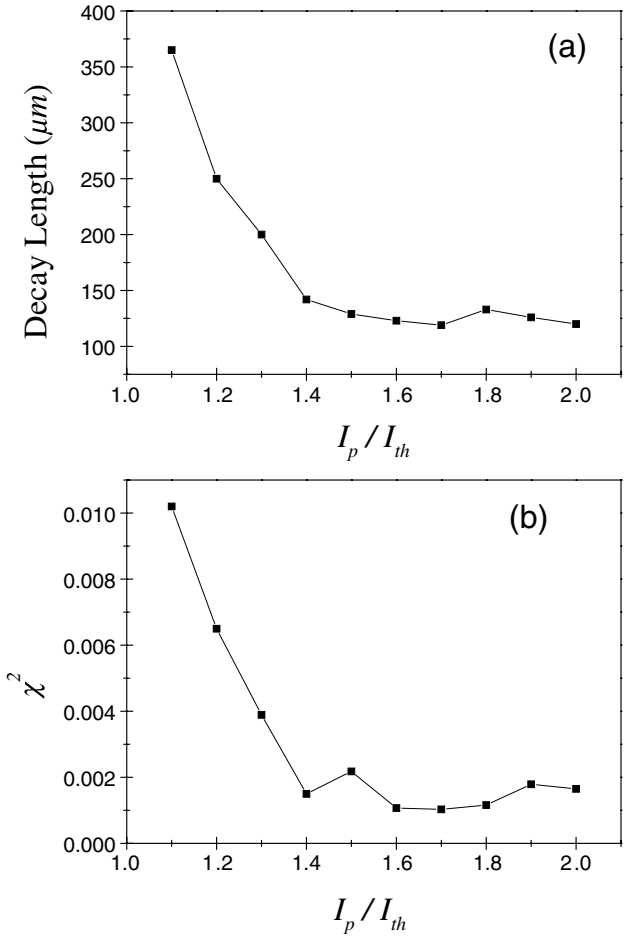

Figure 15. (a) The decay length as a function the pump intensity I_p normalized to the threshold value I_{th}. (b) The fitting error χ^2 versus the normalized pump intensity I_p/I_{th}.

The decay length of a lasing mode is also independent of the excitation area. We varied the diameter of the pump spot at the sample surface from 50 to 400 μm by adding two lens and an aperture to the optical path of the pump beam. When the incident pump power was fixed and the excitation area was reduced, some modes with longer decay length stopped lasing, while other modes with shorter decay length started lasing. This is because the smaller modes have more spatial overlap with the gain volume when the diameter of the pump spot is smaller than the decay length. The effective gain for the smaller states is higher, thus it is easier for them to lase. However, some states kept lasing as the pump area was varied. Their decay lengths did not change with the pump area.

Therefore, the decay length reflects the spatial extent of a lasing mode. As the transport mean free path decreases, the average decay length gets shorter, and the lasing modes become smaller. Now we can understand the critical pump area observed in figure 12. When the pump area is smaller than the size of the lasing mode, the lasing state and the excitation volume have incomplete overlap in the transverse direction (parallel to the sample surface). Enlarging the pump area increases the spatial overlap of the gain volume and the lasing mode. The increase of the effective gain for the lasing mode leads to a reduction in the lasing threshold. Once the pump

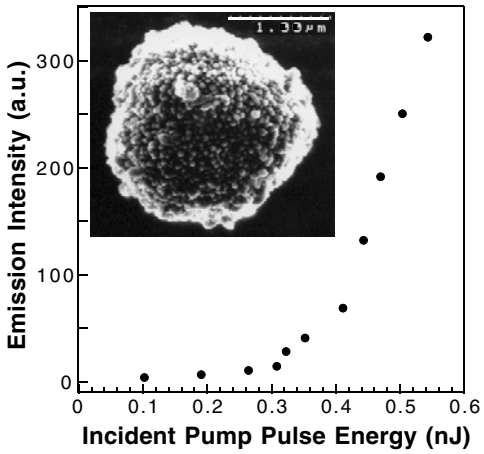

Figure 16. Spectrally integrated intensity of emission from the ZnO cluster versus the incident pump pulse energy. The inset is the SEM image of the ZnO cluster.

area covers the entire lasing mode, the effective gain for the lasing mode no longer increases with the pump area, thus the lasing threshold does not depend on the pump area any longer. In the samples with shorter l_t, the lasing modes are smaller; so are the critical pump areas.

3.4. Micro random laser

After improving the spatial resolution of the spectrally resolved speckle technique, we found the dimension of lasing modes can be as small as a couple of microns in closely packed ZnO nanoparticles ($1 < k_e l_t < 10$). Therefore, when the random system moves toward the localization threshold ($k_e l_t = 1$), the size of the lasing states approaches the optical wavelength. This result illustrates that strong optical scattering not only supplies coherent feedback for lasing, but also leads to spatial confinement of laser light in a micrometre-sized volume. Utilizing this mechanism of optical confinement, we fabricated microlasers with disordered media (Cao *et al* 2000c).

To fabricate a micrometre-sized random medium, ZnO nanoparticles were agglomerated to form clusters whose size varied from half a micron to a few microns. The inset of figure 16 is the SEM image of a typical ZnO cluster. The size of the cluster was about 1.7 μm. It contained roughly 20 000 ZnO nanoparticles. The ZnO cluster was optically pumped by the third harmonic of a pulsed Nd:YAG laser. The pump light was focused by a microscope objective lens onto a single cluster. We simultaneously measured the spectrum of emission from the cluster and imaged the spatial distribution of the emitted light intensity across the cluster.

At low pump intensity, the emission spectrum consisted of a single broad spontaneous emission speak (figure 17(a)). Its FWHM was 12 nm. The spatial distribution of the spontaneous emission intensity was uniform across the cluster (figure 17(b)). When the pump intensity exceeded a threshold, a sharp peak emerged in the emission spectrum (figure 17(c)). Its FWHM is 0.2 nm. Simultaneously, a couple of bright spots appeared in the image of the emitted light distribution in the cluster (figure 17(d)). When the pump intensity was increased further, a second sharp peak emerged in the emission spectrum (figure 17(e)). Correspondingly, additional bright spots appeared in the image of the emitted light distribution (figure 17(f)).

The curve of the total emission intensity as a function of the pump intensity in figure 16 exhibits a distinct slope change at the threshold where sharp spectral peaks and

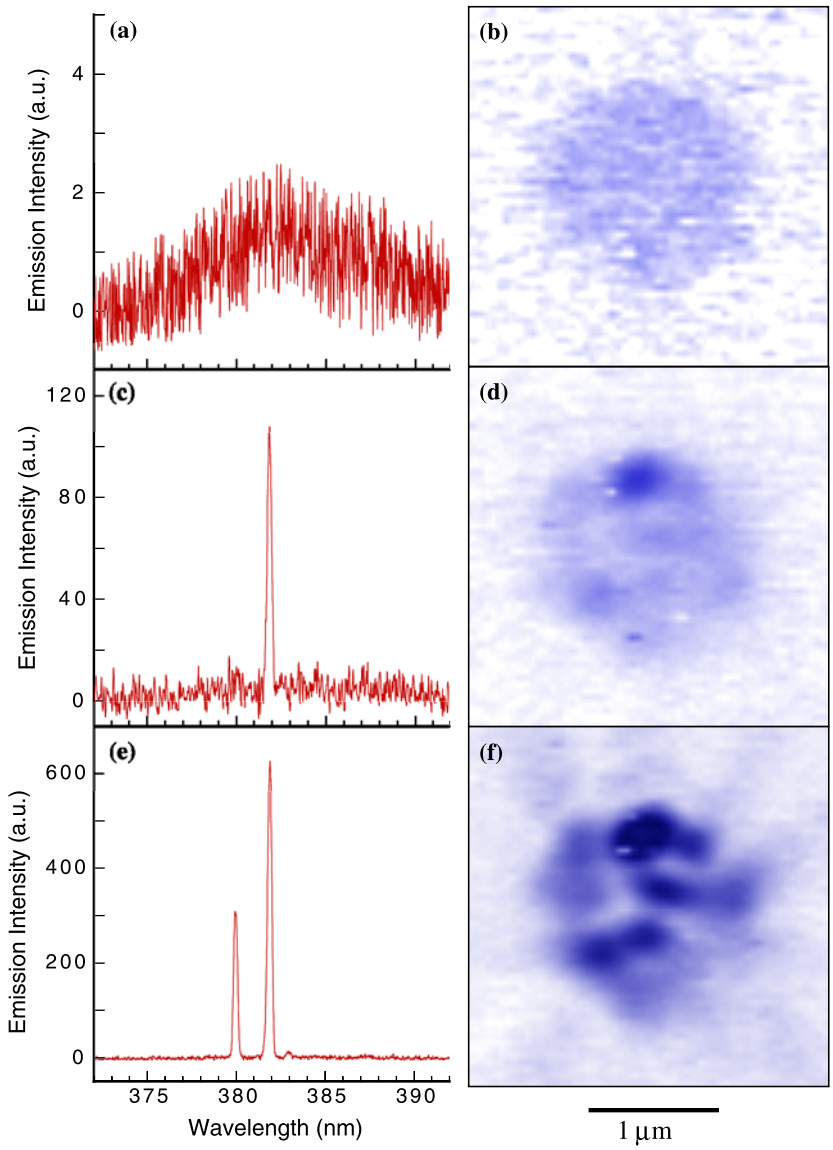

Figure 17. (a), (c) and (e) are the spectra of emission from the ZnO cluster shown in figure 16. (b), (d) and (f) are the corresponding spatial distributions of emission intensity in the cluster. The incident pump pulse energy is 0.26 nJ for (a) and (b), 0.35 nJ for (c) and (d) and 0.50 nJ for (e) and (f).

bright spots appear. Well above the threshold, the total emission intensity increases almost linearly with the pump intensity. These data suggest lasing oscillation in the micrometre-sized cluster. The incident pump pulse energy at the lasing threshold is ∼0.3 nJ. Note that less than ∼1% of the incident pump light is absorbed. The rest is scattered.

Since the cluster is very small, optical reflection from the boundary of the cluster might have some contribution to light confinement in the cluster. However, the laser cavity is not formed by total internal reflection at the boundary. Otherwise the spatial pattern of laser light

would be a bright ring near the edge of the cluster (Taniguchi *et al* 1996). We believe the 3D optical confinement in a micrometre-sized ZnO cluster is achieved through disorder-induced scattering and interference. Since the interference effect is wavelength sensitive, only light at certain wavelengths can be confined in a cluster. In another cluster of different particle configuration, light at different wavelengths is confined. Because optical confinement is not caused by light reflection at the surface of a cluster but by scattering inside the cluster, we achieved lasing in clusters with irregular shapes and rough surfaces.

Let me compare the micro random laser with other types of microlaser. Over the past decade, several types of microlaser have been developed. The key issue for a microlaser is to confine light in a small volume with dimension on the order of optical wavelength. In the vertical cavity surface emitting laser, light is confined by two distributed Bragg reflectors (Jewell *et al* 1991). The microdisc laser utilizes total internal reflection at the edge of a high-index disc to form whispering-gallery modes (McCall *et al* 1992). In the 2D photonic bandgap defect mode laser, light confinement is realized through Bragg scattering in a periodic structure (Painter *et al* 1999). The fabrication of these microlasers requires expensive crystal growth and nanofabrication facilities. In the micro random laser, the optical confinement is achieved through disorder-induced scattering and interference. The fabrication of the micro random laser is much easier and cheaper than that of most microlasers. The frequencies of micro random lasers cannot be well controlled as compared to other types of microlaser. In fact, the lasing frequencies, depending on random particle configurations, are fingerprints of individual clusters.

3.5. A different type of random laser cavity

In the last few sections, the formation of random laser cavities is attributed to the recurrent scattering and interference effect. This mechanism applies to random media with discrete scatterers and strong short-range disorder. A different type of resonant cavity can be formed by smooth long-range inhomogeneity in a weakly disordered medium (Polson *et al* 2002).

Vardeny and co-workers conducted extensive experimental studies on random lasing in weakly disordered media such as π-conjugated polymer films (Frolov *et al* 1999a, Polson *et al* 2001b), organic-dye-doped gel films (Frolov *et al* 1999b) and synthetic opals infiltrated with π-conjugated polymers and dyes (Frolov *et al* 1999b, Yoshino *et al* 1999, Polson *et al* 2001a). They performed the power Fourier transform (PFT) of the laser emission spectrum to obtain the typical length of lasing cavities (Polson *et al* 2002). In the weakly disordered polymer films ($l_t \gg \lambda$), the cavity length was much longer than the transport mean free path. Although the PFT of individual random lasing spectra exhibited position-specific multipeak structures, averaging the PFTs over the sample positions did not smear these features, but on the contrary yielded a series of distinct transform peaks. Moreover, the shape of the averaged PFT was universal, i.e., increasing the disorder and correspondingly reducing l_t did not change this shape: the average of the PFT spectra at different l_t scaled with l_t to a universal curve. Polson *et al* (2002) suggested that the large resonators are formed due to the long-range inhomogeneities of the refractive index. A plausible microscopic origin of these inhomogeneities is the fluctuation of the polymer film thickness. Light is trapped in a high-index region, which is much larger than l_t and λ, by total internal reflection at the boundary of this region. The ability of most random resonators to trap light is suppressed by the short-range disorder. The dramatic consequence of this suppression is that the resonators that 'survive' the short-range disorder are sparse, and consequently almost identical. Raikh *et al* developed a theory based only on the assumption that the random resonators are exponentially sparse without specifying the shape of the resonators. They showed that this assumption was enough to reproduce the universal shape of the averaging PFT.

4. Random laser with coherent feedback—theory

Obviously the theoretical models set up for the random laser with incoherent feedback cannot be applied to the random laser with coherent feedback. What is calculated in those models is light intensity instead of EM field. The phase of the light field is neglected, thus these models do not include the interference effect which is essential to coherent feedback. In order to model the random laser with coherent feedback, we must replace the diffusion equation for light intensity by the Maxwell equations for EM field (Cao *et al* 2000b). Lately, several theoretical models have been set up for the random laser with coherent feedback, e.g., the time-dependent theory (Jiang and Soukoulis 2000), the collective modes of resonant scatterers (Burin *et al* 2001), the prelocalized modes in diffusive media (Apalkov *et al* 2002), the Anderson model (Patra 2003) etc. In this section, a brief introduction to some of the theoretical work is presented.

4.1. Chaotic laser theory

The chaotic cavity laser is a special kind of random laser. In a chaotic cavity, the dynamics is chaotic due to the irregular shape of the cavity and/or scatterers placed at random positions inside the cavity. A typical chaotic cavity has one or a few openings whose dimension is smaller than the wavelength. Photons are trapped inside the cavity long enough to ergodically explore the entire cavity volume. Misirpashaev and Beenakker (1998) calculated the statistical distribution of the lasing threshold in chaotic cavities. The mean value of pumping rate at the lasing threshold is well below the pumping rate needed to compensate the average cavity loss. The average number of non-competing lasing modes is proportional to the square root of the pumping rate. However, mode competition reduces the number of lasing modes because of the spatial hole burning. The laser linewidth is enhanced above the Schawlow–Townes value by the Petermann factor K, owing to the non-orthogonality of the cavity modes (Patra *et al* 2000, Frahm *et al* 2000, Schomerus *et al* 2000). Beenakker (1998) computed the statistics of the emitted radiation by the input–output relation below the lasing threshold where gain saturation is negligible. The ASE exhibits excessive noise, which increases with optical gain and diverges at the lasing threshold. The origin of the excessive noise lies in the presence of a large number of overlapping cavity modes and a broad distribution of the corresponding scattering strengths. Taking into account gain nonlinearity above the lasing threshold, Hackenbroich *et al* (2001) derived the photon statistics of a single-mode chaotic laser. The distribution of the mean photocount over an ensemble of modes changes qualitatively at the lasing transition, and displays up to three peaks above the lasing threshold. Patra (2002) studied the effect of mode competition on noise of a multi-mode chaotic laser. The amount of photon number fluctuation is increased above the Poissonian value by an amount that depends on the number of lasing modes. Despite extensive theoretical studies, experimental work is sparse due to the difficulty in fabricating chaotic cavities with openings smaller than the optical wavelength. A recent wave chaos experiment in a macroscopic open resonator brings hope for the experimental realization of a chaotic cavity laser (Dingjan *et al* 2002). Nevertheless, most random laser experiments have been performed on open systems with strong coupling to the outside reservoir. The emitted light can no longer explore the entire random medium ergodically before escaping through the boundary. Several theories were developed to deal with such random systems.

4.2. Time-dependent theory

The time-dependent theory for the random laser couples the Maxwell equations with the rate equations of electronic population (Jiang and Soukoulis 2000). The gain medium is the four-level electronic material. Electrons are pumped from level 0 to 3, then relax quickly (with time constant τ_{32}) to level 2. Levels 2 and 1 are the upper and lower levels of the lasing transition at

frequency ω_a. After radiative decay (with time constant τ_{21}) from level 2 to 1, electrons relax rapidly (with time constant τ_{10}) from level 1 back to level 0. The populations in four levels (N_3, N_2, N_1, N_0) satisfy the following rate equations:

$$\begin{aligned}
\frac{\mathrm{d}N_3(\vec{r},t)}{\mathrm{d}t} &= P_r(t)N_0(\vec{r},t) - \frac{N_3(\vec{r},t)}{\tau_{32}},\\
\frac{\mathrm{d}N_2(\vec{r},t)}{\mathrm{d}t} &= \frac{N_3(\vec{r},t)}{\tau_{32}} + \frac{\vec{E}(\vec{r},t)}{\hbar\omega_a}\cdot\frac{\mathrm{d}\vec{P}(\vec{r},t)}{\mathrm{d}t} - \frac{N_2(\vec{r},t)}{\tau_{21}},\\
\frac{\mathrm{d}N_1(\vec{r},t)}{\mathrm{d}t} &= \frac{N_2(\vec{r},t)}{\tau_{21}} - \frac{\vec{E}(\vec{r},t)}{\hbar\omega_a}\cdot\frac{\mathrm{d}\vec{P}(\vec{r},t)}{\mathrm{d}t} - \frac{N_1(\vec{r},t)}{\tau_{10}},\\
\frac{\mathrm{d}N_0(\vec{r},t)}{\mathrm{d}t} &= \frac{N_1(\vec{r},t)}{\tau_{10}} - P_r(t)N_0(\vec{r},t).
\end{aligned} \tag{23}$$

$P_r(t)$ represents the external pumping rate. $\vec{P}(\vec{r},t)$ is the polarization density that obeys the equation

$$\frac{\mathrm{d}^2\vec{P}(\vec{r},t)}{\mathrm{d}t^2} + \Delta\omega_a\frac{\mathrm{d}\vec{P}(\vec{r},t)}{\mathrm{d}t} + \omega_a^2\vec{P}(\vec{r},t) = \frac{\gamma_r}{\gamma_c}\frac{e^2}{m}[N_1(\vec{r},t) - N_2(\vec{r},t)]\vec{E}(\vec{r},t). \tag{24}$$

ω_a and $\Delta\omega_a$ represent the centre frequency and linewidth of the atomic transition from level 2 to 1. $\gamma_r = 1/\tau_{21}$, $\gamma_c = e^2\omega_a^2/6\pi\varepsilon_0 mc^3$, where e and m is electron charge and mass. $\vec{P}(\vec{r},t)$ introduces gain to the Maxwell equations:

$$\nabla\times\vec{E}(\vec{r},t) = -\frac{\partial\vec{B}(\vec{r},t)}{\partial t}, \tag{25}$$

$$\nabla\times\vec{H}(\vec{r},t) = \varepsilon(\vec{r})\frac{\partial\vec{E}(\vec{r},t)}{\partial t} + \frac{\partial\vec{P}(\vec{r},t)}{\partial t}, \tag{26}$$

where $\vec{B}(\vec{r},t) = \mu\vec{H}(\vec{r},t)$. The disorder is described by the spatial fluctuation of the dielectric constant $\varepsilon(\vec{r})$. The Maxwell equations are solved with the finite-difference time-domain (FDTD) method (Taflove 1995) to obtain the EM field distribution in the random medium. The Fourier transform of $\vec{E}(\vec{r},t)$ gives the local emission spectrum. To simulate an open system, the random medium has a finite size and it is surrounded by air. The surrounding air is terminated by strongly absorbing layers, e.g. the uniaxial perfectly matched layers that absorb all the light escaping through the boundary of the random medium (Sacks *et al* 1995). Within a semiclassical framework, the spontaneous emission can be included in the Maxwell equations as a noise current.

Jiang and Soukoulis simulated the lasing phenomenon in a 1D random system with the time-dependent theory. A critical pumping rate exists for the appearance of lasing peaks in the spectrum. The number of lasing modes increases with the pumping rate and the length of the system. When the pumping rate increases even further, the number of lasing modes does not increase any more, but saturates to a constant value, which is proportional to the system size for a given randomness. This saturation is caused by spatial repulsion of lasing modes that results from gain competition and spatial localization of the lasing modes. When a mode lases, it depletes local gain and only those modes far enough from it can lase. Because every lasing mode dominates a local region and is separated from other lasing modes, only a limited number of lasing modes can exist in a finite-sized random medium. This prediction was later confirmed experimentally (Ling *et al* 2001). The time-dependent theory is especially suitable for the simulation of laser dynamics. Soukoulis *et al* (2002) simulated the dynamic response and relaxation oscillation in random lasers. The simulation reproduced most of the experimental observations and provided an understanding of the dynamic response of the random laser.

Vanneste and Sebbah calculated the spatial profile of lasing modes in 2D random media with the above method (Vanneste and Sebbah 2001, Sebbah and Vanneste 2002). They compared the passive modes of a 2D random system with the lasing modes when gain is activated. In the strong-localization regime, the lasing modes are identical to the passive modes without gain. When the external pump is focused, the lasing modes change with the location of the pump, in agreement with the experimental observation. Therefore, local pumping of the system allows selective excitation of individual localized modes. Jiang and Soukoulis (2002) also showed that a knowledge of the density of states and the eigenstates of a random system without gain, in conjuction with the frequency profile of the gain, can accurately predict the mode that will lase first.

The advantage of the time-dependent theory is that it can simulate lasing in a real sample after inputting the structure and material information. The numerical simulation gives the lasing spectra, the spatial distribution of lasing modes and the dynamic response that can be compared directly with the experimental measurement. The problem is that simulation of large samples requires too much computing power and the running time cannot be too long. So far the numerical simulations have been carried out only in 1D and 2D systems, even though the method can be applied to 3D systems. Furthermore, the simulation must be done for thousands of samples with different configurations before any statistical conclusion can be drawn.

4.3. Analytical approach

Analytical approaches were taken to derive the conditions for coherent steady-state laser oscillation in random media (Herrmann and Wilhelmi 1998, Burin *et al* 2002, Jiang and Soukoulis 2002). In analogy to the Fabry–Perot laser, the threshold conditions for coherent lasing in a 1D random system include both the steady-state round-trip gain condition and the round-trip phase shift condition.

The semiclassical laser theory can be generalized to the random laser (Jiang and Soukoulis 2002). The slowly varying approximation gives $E(\vec{r}, t) = E(t)\phi(\vec{r})\exp(-\mathrm{i}\omega t)$. The real and imaginary parts of the Maxwell equation of $E(\vec{r}, t)$ become

$$\nabla^2\phi(\vec{r}) + \mu_0[\varepsilon(\vec{r}) + \varepsilon_0\chi'(\vec{r}, \omega)]\omega^2\phi(\vec{r}) = 0, \tag{27}$$

$$\frac{\mathrm{d}E(t)}{\mathrm{d}t} = \left(-\langle\chi''(\omega)\rangle - \frac{1}{Q}\right)\frac{\varepsilon_0\omega E(t)}{2\langle\varepsilon\rangle}, \tag{28}$$

where $\langle\varepsilon\rangle$ and $-\langle\chi''\rangle$ represent the spatially averaged dielectric constant and gain. Equation (27) determines the lasing frequency ω, the field distribution $\phi(\vec{r})$ and the quality factor Q. The term $\varepsilon_0\chi'(\vec{r}, \omega)$ causes a shift of the lasing frequency from the eigenfrequency of the passive system (the pulling effect). When Q is large, a small gain is needed to reach the lasing threshold. Then $\chi'(\vec{r}, \omega) \ll 1$, the pulling effect is very weak. The lasing frequency is almost the same as the eigenfrequency, and the wavefunction of the lasing mode is nearly identical to the eigenfunction of the passive system. Equation (28) is the time-dependent amplitude equation; it sets the threshold condition $-\langle\chi''(\omega)\rangle = 1/Q$. Equation (28) also gives the stable amplitude of the field above the lasing threshold.

4.4. Quantum theory

Quantum theory is needed to understand the quantum statistical properties of random lasers. Standard quantum theory for lasers only applies to quasi-discrete modes and cannot account for lasing in the presence of overlapping modes. In a random medium, the character of lasing modes depends on the amount of disorder. Weak disorder leads to a poor confinement of light

and to strongly overlapping modes. Statistics naturally enters the random scattering theory pioneered by Beenakker (Beenakker 1998, Patra and Beenakker 1999, 2000, Mishchenko *et al* 2001), but that approach is restricted to linear media and cannot describe the random laser above the lasing threshold. Hackenbroich *et al* (2002) developed a quantization scheme for optical resonators with overlapping modes. Feshbach's projector technique, previously applied to condensed matter physics, was employed to quantize the EM field. The EM field Hamiltonian of open resonators reduces to the well known system-and-bath Hamiltonian of quantum optics. Upon including an amplifying medium, it could serve as a starting point for the quantum theory of the random laser.

5. Interplay of light localization and coherent amplification

The study of the random laser is closely related to that of light localization. The interplay of light localization and coherent amplification has attracted much interest and study.

The effect of gain on CBS (weak localization) was studied both theoretically (Zyuzin 1994, Deng *et al* 1997, Tutov and Maradudin 1999) and experimentally (Wiersma *et al* 1995b, de Oliveira *et al* 1996). The shape of the backscattering cone is determined by the transport distance of light in the medium. The intensity in an amplifying medium grows exponentially with the path length. Consequently, gain enhances the long path lengths that constitute the top of the backscattering cone. Thus, a larger contribution of long paths yields a sharper and narrower cone as compared to the passive medium.

The effect of amplification on light reflection and transmission in a random system has been extensively investigated and compared with the effect of absorption (Pradhan and Kumar 1994, Zhang 1995, Zyuzin 1995, Beenakker 1996, Paasschens *et al* 1996, Burkov and Zyuzin 1996, 1997, Freilikher *et al* 1997, Jiang and Soukoulis 1999a, 1999b). These studies were carried out mostly in 1D or quasi-1D systems with time-independent theory. Optical gain is introduced through the imaginary part of the refractive index. Below the lasing threshold, coherent amplification enhances not only light reflection but also transmission at resonant frequencies. However, non-resonant transmission is suppressed. Moreover, amplification leads to an increase in the fluctuation of the transmissivity T and reflectivity R. On approaching the lasing threshold, both the mean value and the variance of T and R diverge. Above the threshold, the time-independent theory no longer works, and it must be replaced by time-dependent theory. The lasing threshold is related to transmission in a 1D random system (Burin *et al* 2002). More specifically, in the localization regime, the lasing threshold is defined by the transmission through the passive system. Thus, the average lasing threshold depends exponentially on the size of the random system. Moreover, the lasing threshold fluctuates strongly from configuration to configuration.

So far, the numerical simulation on a coherent random laser has been conducted only in 1D or 2D random systems (Li *et al* 2001, Jiang and Soukoulis 2000, Burin *et al* 2001, Vanneste and Sebbah 2001, Patra 2003). The characteristics of lasing modes in 3D random media are not fully understood. Theoretically, for a 3D random medium when $l_t > \lambda$, the system is delocalized and the eigenmodes are expected to extend over the entire sample. However, the experimental measurement shows that the size of individual lasing modes was much smaller than that of the entire sample even when $l_t \gg \lambda$. Thus, the lasing modes do not seem to be extended states. One possible explanation is that there exist some prelocalized modes with anomalously low loss (Apalkov *et al* 2002). These modes are very rare in the diffusive regime ($k_e l_t \gg 1$). They are analogous to the prelocalized electronic states in diffusive conductors that are responsible for the long-time asymptotics of the current relaxation (Altshuler *et al* 1991). Apalkov *et al* (2002) calculated the likelihood of prelocalized modes and found it

depends crucially on the size of the scatterers, or, more precisely, on the correlation radius of the disorder. Since the number of prelocalized modes is much less than that of the extended modes, the transport properties are dominated by extended modes. Therefore, it is hard to probe the prelocalized modes in the transmission measurement. However, when optical gain is introduced to a random medium, the prelocalized modes are preferentially amplified because of their long lifetime. Photons in the prelocalized modes stay longer in the gain medium, thus they experience more amplification. As optical gain increases further, the prelocalized modes lase first because of their lower decay rates. Once the prelocalized modes lase, their intensities are much higher than those of the extended modes. Thus, they dominate the emission spectrum and the field pattern. The lasing peaks in the emission spectrum reveal the frequencies of the prelocalized modes, while the lasing threshold pumping rates reflect their lifetimes. The spatial distribution of laser intensity tells the positions and spatial profiles of the prelocalized modes. Therefore, by introducing optical gain to induce lasing in the prelocalized modes, we can directly probe them for the first time (Cao *et al* 2002).

It is well known that optical absorption hinders photon localization because it suppresses the interference of scattered light. Optical amplification, which has the opposite effect of absorption, should facilitate Anderson localization of light. So far, the studies of light localization have been conducted on passive random media. The proximity of a random system to the localization threshold is described by the Thouless number $\delta \equiv \delta\nu/\Delta\nu$, where $\delta\nu$ is the level width and $\Delta\nu$ is the level spacing. The Thouless criterion, $\delta = 1$, marks the onset of Anderson localization (Thouless 1977). However, it is not clear what the criterion is for Anderson localization in an active random medium. The average level width $\delta\nu$ is identified with the field correlation width (Genack 1990). In the presence of gain, the level width is reduced; so is the Thouless number. However, when the gain exceeds the threshold of lasing with coherent feedback, the spectral field correlation function is dominated by the lasing modes with extremely narrow linewidth. The drastic decrease of the field correlation width $\delta\nu$ would bring the Thouless number below unity. This seems to suggest that the Thouless criterion for Anderson localization cannot be used in the case of lasing. Recently a new criterion has been developed for photon localization in an absorbing random medium (Chabanov *et al* 2000). Chabanov *et al* showed that the variance of transmission fluctuation accurately reflects the extent of localization. Unfortunately this criterion does not seem to hold for active random media, because the variance of transmission fluctuation diverges at the lasing threshold. Of course, gain saturation would prevent the divergence; nevertheless, the transmission fluctuation increases dramatically above the lasing threshold. Hence, the criterion for light localization in an active random medium remains to be developed.

6. Applications of the random laser

The random laser is a non-conventional laser whose feedback mechanism is based on random scattering, as opposed to the reflective feedback by the mirrors of a conventional laser. This alternative feedback mechanism has important application to lasers in the spectral regime where an efficient reflective element is not available, e.g., UV laser, x-ray laser. The UV random laser has already been realized with ZnO powder, polycrystalline films and nanowire arrays (Cao *et al* 1998, 1999c, Mitra and Thareja 1999, Thareja and Mitra 2000, Huang *et al* 2001). Furthermore, the low fabrication cost, sample specific wavelength of operation, small size, flexible shape and substrate compatibility of random laser lead to many potential applications. For example, a thin layer of laser paint can be coated on screws, nuts, bolts and manufactured parts for machine-vision application (Lawandy 1994). In the area of search and rescue, the painted-on laser may provide a rugged and low-cost method of identification

for downed ships, aircraft and satellites. In the medical arena, the random laser has potential application to photodynamic therapy and tumour detection. The micro random laser may play the crucial role of an active element or miniature light source in integrated photonic circuits (Wiersma 2000). It can also be used to monitor the flow of liquids by adding a small number of nanoparticle clusters to the liquid and detecting their laser emission over a large flow distances. The specific wavelength of operation, depending on the configuration of scatterers, makes the random laser suitable for document encoding and material labelling.

For some applications, the current threshold of the random laser is too high. Zacharakis *et al* (2002) explored two-photon pumping for the random laser to reduce the threshold. Weak two-photon absorption allows deeper penetration of the pump light into the random medium, and results in better confinement of the emitted light (Burin *et al* 2003). We proposed another scheme to reduce the lasing threshold: incorporating some degree of order into an active random medium (Chang *et al* 2003, Yamilov and Cao 2003). Shkunov *et al* (2001) observed both photonic lasing and random lasing in dye-infiltrated opals. However, random lasing had a higher threshold than photonic lasing. We numerically simulated lasing in a random system with a variable degree of order. When disorder is introduced into a perfectly ordered system, the lasing threshold is reduced. At a certain degree of disorder the lasing threshold reaches a minimum (Chang *et al* 2003). In other words, there exists an optimum degree of order/disorder for lasing, where the lasing threshold is comparable (within a factor of two) to the threshold of a single-defect photonic bandgap laser. We mapped out the transition from full order to complete disorder, and identified five scaling regimes for the mean lasing threshold versus the system size L (Yamilov and Cao 2003). For increasing degree of disorder, the five regimes are (a) photonic band-edge, $1/L^3$, (b) transitional super-exponential, (c) bandgap-related exponential, (d) diffusive, $1/L^2$, and (e) disorder-induced exponential. These predictions remain to be confirmed experimentally.

Unlike the conventional lasers with directional output, laser emission from the random media can be observed in all directions (Cao *et al* 1999b). The isotropic output of a random laser is useful for some applications like displays, but in other applications directional output is desired. Shukri and Armstrong (2000) observed directional emission in the backward direction of the pump beam in a dye solution. Alencar *et al* (2001) exploited the enhancement of directionality due to surface plasmon excitation provided by the contact of the polymer sample with a thin metallic film. We utilized external feedback to reduce the lasing threshold and control the output direction of laser emission (Cao *et al* 1999a).

So far most random lasers are pumped optically. Some applications such as flat-panel, automotive and cockpit displays require electrical pumping. Recently, electrically pumped continuous-wave laser action was reported in rare-earth-metal-doped dielectric nanophosphors and Nd-doped δ-alumina nanopowders (Williams *et al* 2001, Li *et al* 2002).

Last, but not least, the research on the random laser also benefits other research fields. For example, adding optical gain to a random medium creates a new path to study wave transport and localization. Because the random lasing modes are eigenstates of a random system, the interaction of the lasing modes reflects the interaction among the eigenstates. Lately, we have observed the coupling of random lasing modes (Cao *et al* 2003). From this we gained information on the interaction among eigenmodes of a random system. Such knowledge is crucial to understanding the escape channels for photons in an eigenstate, that is important to the localization theory. Moreover, the random laser offers an opportunity to study the interplay between nonlinearity and localization. Nonlinear optical effects are significant in the random laser owing to its high intensity and resonance enhancement. Noginov *et al* (1998a) demonstrated second-harmonic generation in a mixture of powders of laser and frequency doubling materials. Our recent study on the dynamic nonlinear effect in a random laser

illustrates that the third-order optical nonlinearity modifies both the eigen-frequency and eigen-wavefunction of a random system (Liu *et al* 2003). As Letokhov's work showed, the study of the random laser improves our understanding of galaxy masers and stellar lasers whose feedback is caused by scattering (Letokhov 1972, 1996).

Acknowledgments

I wish to thank my co-workers on the study of random lasers. Drs J Y Xu, Y Ling and Y G Zhao and Professor Prem Kumar contributed to the experimental work on random lasers. Drs A L Burin, A Yamilov, B Liu and S-H Chang and Professors S T Ho and M A Ratner conducted theoretical studies of random lasers. Professor R P H Chang and his students E W Seelig, X Liu and H C Ong fabricated ZnO nanoparticles and polycrystalline films. We enjoyed the fruitful collaboration with Professor C M Soukoulis and Dr Xunya Jiang on the simulation of the random laser. Stimulating discussions with Professors V M Letokhov, S John, Z V Vardeny, A Z Genack, M E Raikh, L Deych, M A Noginov, S C Rand, C M de Sterke, D Wiersma, A Taflove, A A Asatryan, M Patra and Ch M Briskina are acknowledged. Our research programme was partly sponsored by the National Science Foundation through the grants ECS-9877113 and DMR-0093949, and by the David and Lucille Packard Foundation, the Alfred P Sloan Foundation and Northwestern University Materials Research Center.

References

Alencar M A R C, Gomes A S L and de Araujo C B 2001 *Quantum Electronics and Laser Science Conf.* technical digest p 173
Altshuler B L, Kravtsov V E and Lerner I V 1991 *Mesoscopic Phenomena in Solids* ed B L Altshuler, P A Lee and R A Webb (Amsterdam: North-Holland)
Ambartsumyan R V, Basov N G, Kryukov P G and Letokhov V S 1966 *IEEE J. Quantum Electron.* **2** 442
Ambartsumyan R V, Basov N G, Kryukov P G and Letokhov V S 1967a *Sov. Phys.–JETP* **24** 1129
Ambartsumyan R V, Basov N G, Kryukov P G and Letokhov V S 1967b *Sov. Phys.–JETP* **24** 481
Ambartsumyan R V, Basov N G and Letokhov V S 1968 *Sov. Phys.–JETP* **26** 1109
Ambartsumyan R V, Bazhulin S P, Basov N G and Letokhov V S 1970 *Sov. Phys.–JETP* **31** 234
Apalkov V M, Raikh M E and Shapiro B 2002 *Phys. Rev. Lett.* **89** 016802
Auzel F and Goldner P 2000 *J. Alloys Compounds* **300** 11
Balachandran R M and Lawandy N M 1995 *Opt. Lett.* **20** 1271
Balachandran R M and Lawandy N M 1996 *Opt. Lett.* **21** 1603
Balachandran R M and Lawandy N M 1997 *Opt. Lett.* **22** 319
Balachandran R M, Perkins A E and Lawandy N M 1996 *Opt. Lett.* **21** 650
Beckering G, Zilker S J and Haarer D 1997 *Opt. Lett.* **22** 1427
Beenakker C W J 1996 *Phys. Rev. Lett.* **76** 1368
Beenakker C W J 1998 *Phys. Rev. Lett.* **81** 1829
Berger G A, Kempe M and Genack A Z 1997 *Phys. Rev.* E **56** 6118
Briskina Ch M and Li L F 2002 *Laser Phys.* **12** 724
Briskina Ch M, Markushev V M and Ter-Gabrielyan N E 1996 *Quantum Electron.* **26** 923
Burin A L, Ratner M A, Cao H and Chang S-H 2002 *Phys. Rev. Lett.* **88** 093904
Burin A L, Ratner M A and Cao H 2003 *IEEE J. Sel. Top. Quantum Electron.* **9** 124
Burin A L, Ratner M A, Cao H and Chang R P H 2001 *Phys. Rev. Lett.* **87** 215503
Burkov A A and Zyuzin A Yu 1996 *JETP Lett.* **63** 878
Burkov A A and Zyuzin A Yu 1997 *Phys. Rev.* B **55** 5736
Cao H, Jiang X, Ling Y, Xu J Y and Soukoulis C M 2003 *Preprint* cond-mat/0301461
Cao H, Ling Y, Xu J Y and Burin A L 2002 *Phys. Rev.* E **66** R25601
Cao H, Ling Y, Xu J Y, Cao C Q and Kumar P 2001 *Phys. Rev. Lett.* **86** 4524
Cao H, Xu J Y, Chang S-H and Ho S T 2000a *Phys. Rev.* E **61** 1985
Cao H, Xu J Y, Chang S-H, Ho S T, Seelig E W, Liu X and Chang R P H 2000b *Phys. Rev. Lett.* **84** 5584
Cao H, Xu J Y, Seelig E W and Chang R P H 2000c *Appl. Phys. Lett.* **76** 2997
Cao H, Zhao Y G, Liu X, Seelig E W and Chang R P H 1999a *Appl. Phys. Lett.* **75** 1213
Cao H, Zhao Y G, Ong H C and Chang R P H 1999b *Phys. Rev.* B **59** 15107

Cao H, Zhao Y G, Ong H C, Ho S T, Dai J Y, Wu J Y and Chang R P H 1998 *Appl. Phys. Lett.* **73** 3656
Cao H, Zhao Y G, Ong H C, Ho S T, Seelig E Q, Wang Q H and Chang R P H 1999c *Phys. Rev. Lett.* **82** 2278
Chabanov A A, Stoytchev M and Genack A Z 2000 *Nature* **404** 850
Chang S-H, Cao H and Ho S T 2003 *IEEE J. Quantum Electron.* **39** 364
de Oliveira P C, McGreevy J A and Lawandy N M 1997 *Opt. Lett.* **22** 895
de Oliveira P C, Perkins A E and Lawandy N M 1996 *Opt. Lett.* **21** 1685
Deng W, Wiersma D and Zhang Z Q 1997 *Phys. Rev.* B **56** 178
Dingjan J, Altewischer E, van Exter M P and Woerdman J P 2002 *Phys. Rev. Lett.* **88** 064101
Frahm K M, Schomerus H, Patra M and Beenakker C W J 2000 *Europhys. Lett.* **49** 48
Freilikher V, Pustilnik M and Yurkevich I 1997 *Phys. Rev.* B **56** 5974
Frolov S V, Vardeny Z V, Yoshino K, Zakhidov A A and Baughman R H 1999a *Phys. Rev.* B **59** R5284
Frolov S V, Vardeny Z V, Yoshino K, Zakhidov A A and Baughman R H 1999b *Opt. Commun.* **162** 241
Genack A Z 1990 *Europhys. Lett.* **11** 733
Genack A Z and Drake J M 1994 *Nature* **368** 400
Gouedard C, Husson D, Sauteret C, Auzel F and Migus A 1993 *J. Opt. Soc. Am.* B **10** 2358
Hackenbroich G, Viviescas C, Elattari B and Haake F 2001 *Phys. Rev. Lett.* **86** 5262
Hackenbroich G, Viviescas C and Haake F 2002 *Phys. Rev. Lett.* **89** 083902
Herrmann J and Wilhelmi B 1998 *Appl. Phys.* B **66** 305
Huang M H, Mao S, Feick H, Yang H, Wu Y, Kind H, Weber E, Russo R and Yang P 2001 *Science* **292** 1897
Jewell J L, Harbison J P, Scherer A, Lee Y H and Florez L T 1991 *IEEE J. Quantum Electron.* **27** 1332
Jiang X and Soukoulis C M 1999a *Phys. Rev.* B **59** 6159
Jiang X and Soukoulis C M 1999b *Phys. Rev.* B **59** R9007
Jiang X and Soukoulis C M 2000 *Phys. Rev. Lett.* **85** 70
Jiang X and Soukoulis C M 2002 *Phys. Rev.* E **65** R025601
John S 1991 *Phys. Today* **44** 32
John S and Pang G 1996 *Phys. Rev.* A **54** 3642
Kuga Y and Ishimaru A 1984 *J. Opt. Soc. Am.* A **8** 831
Lawandy N M 1994 *Photon. Spectra* **28** 119
Lawandy N M and Balachandran R M 1995 *Nature* **373** 204
Lawandy N M, Balachandran R M, Gomes A S L and Sauvain E 1994 *Nature* **368** 436
Lee K and Lawandy N M 2002 *Opt. Commun.* **203** 169
Letokhov V S 1968 *Sov. Phys.–JETP* **26** 1246
Letokhov V S 1972 *IEEE J. Quantum Electron.* **8** 615
Letokhov V S 1996 *Amazing Light* ed R Y Chiao (Berlin: Springer) p 409
Li B, Williams G R, Rand S C, Hinklin T and Laine R M 2002 *Opt. Lett.* **27** 394
Li Q, Ho K M and Soukoulis C M 2001 *Physica* B **296** 78
Lichmanov A A, Briskina Ch M, Markushev V M, Lichmanova V N and Soshchin N P 1998 *J. Appl. Spectrosc.* **65** 818
Ling Y, Cao H, Burin A L, Ratner M A, Liu X and Chang R P H 2001 *Phys. Rev.* A **64** 063808
Liu B, Yamilov A, Ling Y, Xu J Y and Cao H 2003 *Preprint* cond-mat/0301457
Markushev V M, Ter-Garielyan N E, Briskina Ch M, Belan V R and Zolin V F 1990 *Sov. J. Quantum Electron.* **20** 773
Markushev V M, Zolin V F and Briskina Ch M 1986 *Sov. J. Quantum Electron.* **16** 281
Martorell J, Balachandran R M and Lawandy N M 1996 *Opt. Lett.* **21** 239
McCall S L, Levi A F J, Slusher R E, Pearton S J and Logan R A 1992 *Appl. Phys. Lett.* **60** 289
Mishchenko E G, Patra M and Beenakker C W J 2001 *Eur. Phys. J.* D **13** 289
Misirpashaev T Sh and Beenakker C W J 1998 *Phys. Rev.* A **57** 2041
Mitra A and Thareja R K 1999 *Mod. Phys. Lett.* B **23** 1075
Noginov M A, Caulfield H J, Noginova N E and Venkateswarlu P 1995 *Opt. Commun.* **118** 430
Noginov M A, Egarievwe S U, Noginova N E, Caulfield H J and Wang J C 1999 *Opt. Mater.* **12** 127
Noginov M A, Egarievwe S U, Noginova N E, Wang J C and Caulfield H J 1998a *J. Opt. Soc. Am.* B **15** 2854
Noginov M A, Noginova N E, Egarievwe S U, Caulfield H J, Cochrane C, Wang J C, Kokta M R and Paitz J 1998b *Opt. Mater.* **10** 297
Noginov M A, Noginova N E, Egarievwe S U, Caulfield H J, Venkateswarlu P, Thompson T, Mahdi M and Ostroumov V 1996 *J. Opt. Soc. Am.* B **13** 2024
Noginov M A, Noginova N E, Egarievwe S U, Caulfield H J, Venkateswarlu P, Williams A and Mirov S B 1997 *J. Opt. Soc. Am.* B **14** 2153
Paasschens J C J, Misirpashaev T Sh and Beenakker C W J 1996 *Phys. Rev.* B **54** 11887

Painter O, Lee R K, Scherer A, Yariv A, O'Brien J D, Dapkus P D and Kim I 1999 *Science* **284** 1819
Patra M 2002 *Phys. Rev.* A **65** 043809
Patra M 2003 *Phys. Rev.* E **67** 016603
Patra M and Beenakker C W J 1999 *Phys. Rev.* A **60** 4059
Patra M and Beenakker C W J 2000 *Phys. Rev.* A **61** 063805
Patra M, Schomerus H and Beenakker C W J 2000 *Phys. Rev.* A **61** 023810
Polson R C, Chipouline A and Vardeny Z V 2001a *Adv. Mater.* **13** 760
Polson R C, Huang J D and Vardeny Z V 2001b *Synth. Met.* **119** 7
Polson R C, Raikh M E and Vardeny Z V 2002 *C. R. Acad. Sci. Paris* IV **3** 509
Pradhan P and Kumar N 1994 *Phys. Rev.* B **50** 9644
Sacks Z S, Kingsl D M, Lee R and Lee J F 1995 *IEEE Trans. Antennas Propag.* **43** 1460
Schomerus H, Frahm K M, Patra M and Beenakker C W J 2000 *Physica* A **278** 469
Sebbah P and Vanneste C 2002 *Phys. Rev.* B **66** 144202
Sha W L, Liu C-H and Alfano R R 1994 *Opt. Lett.* **19** 1922
Sha W L, Liu C-H, Liu F and Alfano R R 1996 *Opt. Lett.* **21** 1277
Shkunov M N, DeLong M C, Raikh M E, Vardeny Z V, Zakhidov A A and Baughman R H 2001 *Synth. Met.* **116** 485
Shukri M and Armstrong R L 2000 *Appl. Opt.* **39** 4300
Siddique M, Alfano R R, Berger G A, Kempe M and Genack A Z 1996 *Opt. Lett.* **21** 450
Siegman A 1986 *Lasers* (Mill Valley, CA: University Science Books)
Soukoulis C M, Jiang X, Xu J Y and Cao H 2002 *Phys. Rev.* B **65** R041103
Taflove A 1995 *Computational Electrodynamics: the Finite-Difference Time Domain Method* (Boston, MA: Artech)
Taniguchi H, Tanosaki S, Tsujita K and Inaba H 1996 *IEEE J. Quantum Electron.* **32** 1864
Ter-Garielyan N E, Markushev V M, Belan V R, Briskina Ch M, Dimitrova O V, Zolin V F and Lavrov A V 1991a *Sov. J. Quantum Electron.* **21** 840
Ter-Garielyan N E, Markushev V M, Belan V R, Briskina Ch M and Zolin V F 1991b *Sov. J. Quantum Electron.* **21** 32
Thareja R K and Mitra A 2000 *Appl. Phys.* B **71** 181
Thouless D J 1977 *Phys. Rev. Lett.* **39** 1167
Totsuka K, van Soest G, Ito T, Lagendijk A and Tomita M 2000 *J. Appl. Phys.* **87** 7623
Tutov A V and Maradudin A A 1999 *Phys. Rev.* B **60** 12692
van Albada M P and Lagendijk A 1985 *Phys. Rev. Lett.* **55** 2692
van Soest G and Lagendijk A 2002 *Phys. Rev.* E **65** 047601
van Soest G, Poelwijk F J and Lagendijk A 2002 *Phys. Rev. Lett.* **65** 046603
van Soest G, Poelwijk F J, Sprik R and Lagendijk A 2001 *Phys. Rev. Lett.* **86** 1522
van Soest G, Tomita M, Sprik R and Lagendijk A 1999 *Opt. Lett.* **24** 306
Vanneste C and Sebbah P 2001 *Phys. Rev. Lett.* **87** 183903
Wiersma D 2000 *Nature* **406** 132
Wiersma D and Cavalieri S 2001 *Nature* **414** 709
Wiersma D, van Albada M P and Lagendijk A 1995a *Nature* **373** 203
Wiersma D, van Albada M P and Lagendijk A 1995b *Phys. Rev. Lett.* **75** 1739
Wiersma D S and Lagendijk A 1997a *Phys. Rev.* E **54** 4256
Wiersma D S and Lagendijk A 1997b *Phys. World* **10** 33
Williams G R, Bayram S B, Rand S C, Hinklin T and Laine R M 2001 *Phys. Rev.* A **65** 013807
Wolf P E and Maret G 1985 *Phys. Rev. Lett.* **55** 2696
Yamilov A and Cao H 2003 *Preprint* cond-mat/0209680
Yoshino K, Tatsuhara S, Kawagishi Y and Ozaki M 1999 *Appl. Phys. Lett.* **74** 2590
Zacharakis G, Heliotis G, Filippidis G, Anglos D and Papazoglou T G 1999 *Appl. Opt.* **38** 6087
Zacharakis G, Papadogiannis N A, Filippidis G and Papazoglou T G 2000 *Opt. Lett.* **25** 923
Zacharakis G, Papadogiannis N A and Papazoglou T G 2002 *Appl. Phys. Lett.* **81** 2511
Zhang D, Cheng B, Yang J, Zhang Y, Hu W and Li Z 1995a *Opt. Commun.* **118** 462
Zhang W, Cue N and Yoo K M 1995b *Opt. Lett.* **20** 961
Zhang W, Cue N and Yoo K M 1995c *Opt. Lett.* **20** 1023
Zhang Z Q 1995 *Phys. Rev.* B **52** 7960
Zolin V F 2000 *J. Alloys Compounds* **300** 214
Zyuzin A Yu 1994 *Europhys. Lett.* **26** 517
Zyuzin A Yu 1995 *Phys. Rev.* E **51** 5274
Zyuzin A Yu 1998 *JETP* **86** 445
Zyuzin A Yu 1999 *Europhys. Lett.* **46** 160